This article has been accepted for inclusion in a future issue of this journal. Content is final as presented, with the exception of pagination.

MiRS: An All-Weather 1DVAR Satellite Data Assimilation and Retrieval System

Sid-Ahmed Boukabara, Kevin Garrett, Wanchun Chen, Flavio Iturbide-Sanchez, *Member, IEEE*, Christopher Grassotti, Cezar Kongoli, Ruiyue Chen, Quanhua Liu, Banghua Yan, Fuzhong Weng, Ralph Ferraro, Thomas J. Kleespies, and Huan Meng

***Abstract*—A 1-D variational system has been developed to process spaceborne measurements. It is an iterative physical inversion system that finds a consistent geophysical solution to fit all radiometric measurements simultaneously. One of the particularities of the system is its applicability in cloudy and precipitating conditions. Although valid, in principle, for all sensors for which the radiative transfer model applies, it has only been tested for passive microwave sensors to date. The Microwave Integrated Retrieval System (MiRS) inverts the radiative transfer equation by finding radiometrically appropriate profiles of temperature, moisture, liquid cloud, and hydrometeors, as well as the surface emissivity spectrum and skin temperature. The inclusion of the emissivity spectrum in the state vector makes the system applicable globally, with the only differences between land, ocean, sea ice, and snow backgrounds residing in the covariance matrix chosen to spectrally constrain the emissivity. Similarly, the inclusion of the cloud and hydrometeor parameters within the inverted state vector makes the assimilation/inversion of cloudy and rainy radiances possible, and therefore, it provides an all-weather capability to the system. Furthermore, MiRS is highly flexible, and it could be used as a retrieval tool (independent of numerical weather prediction) or as an assimilation system when combined with a forecast field used as a first guess and/or background. In the MiRS, the fundamental products are inverted first and then are interpreted into secondary or derived products such as sea ice concentration, snow water equivalent (based on the retrieved emissivity) rainfall rate, total precipitable water, integrated cloud liquid amount, and ice water path (based on the retrieved atmospheric and hydrometeor products). The MiRS system was implemented operationally at the U.S. National Oceanic and Atmospheric Administration (NOAA) in 2007 for the NOAA-18 satellite. Since then, it has been extended to run for NOAA-19, Metop-A, and DMSP-F16 and F18 SSMI/S. This paper gives an overview of the system and presents brief results of the assessment effort for all fundamental and derived products.**

***Index Terms*—Atmospheric sounding, cloudy and rainy data assimilation, microwave retrieval, surface sensing.**

Manuscript received April 7, 2010; revised March 2, 2011; accepted April 22, 2011. This work was supported by the U.S. National Oceanic and Atmospheric Administration (NOAA) Office of Systems Development (OSD) Product Systems Development Implementation (PSDI). The views expressed here are solely those of the authors and do not constitute a statement of policy, decision, or position on behalf of NOAA or the U.S. Government.

S.-A. Boukabara, F. Weng, R. Ferraro, T. Kleespies, and H. Meng are with the National Oceanic and Atmospheric Administration Center for Satellite Applications and Research, Camp Springs, MD 20746 USA (e-mail: sid.boukabara@noaa.gov; fuzhong.weng@noaa.gov; ralph.r.ferraro@noaa.gov; thomas.j.kleespies@noaa.gov; Huan.Meng@noaa.gov).

K. Garrett, F. Iturbide-Sanchez, C. Grassotti, and R. Chen are with the I.M. Systems Group, Inc., Camp Springs, MD 20746 USA (e-mail: kevin.garrett@noaa.gov; Flavio.Iturbide@noaa.goc; Chris.Grassotti@noaa.gov; Ruiyue.Chen@noaa.gov).

W. Chen and Q. Liu are with Dell, Inc., Camp Springs, MD 20746 USA (e-maul: wanchun.chen@noaa.gov; quanhua.liu@noaa.gov).

C. Kongoli and B. Yan are with the Earth System Science Interdisciplinary Center, University of Maryland, College Park, MD 20740-3823 USA (e-mail: Cezar.Kingoli@noaa.gov; banghua.yan@noaa.gov).

Color versions of one or more of the figures in this paper are available online at http://ieeexplore.ieee.org.

Digital Object Identifier 10.1109/TGRS.2011.2158438

I. INTRODUCTION

THE NUMERICAL weather prediction (NWP) radiance assimilation and the physical retrieval process based on the variational approach are mathematically similar concepts sharing a number of common characteristics: 1) a similar cost function to be minimized; 2) the need to have accurate and representative covariance matrices and mean backgrounds; 3) the reliance on an accurate forward operator to simulate measurements; and 4) the similar issues of convergence, noise estimation, and radiometric bias removal. The Microwave Integrated Retrieval System (MiRS) presented in this paper could be used in both modes, and it relies on the Community Radiative Transfer Model (CRTM) to provide both the simulated radiances and the Jacobians with respect to all geophysical parameters to be inverted, including hydrometeors. The state vector is constrained by a set of covariance matrices generated offline to reduce the null-space and to ensure a physically consistent final solution. The computation of the derivatives (k-matrix) in CRTM is performed using *tangent linear* (TL) and *adjoint* (AD) approaches. When used in absorption-only mode, it is found that convergence of the system is reached globally, even in coastal areas, with pockets of nonconvergence highly correlated to cases of precipitation, presence of ice, and, generally, any situation that the forward operator cannot handle properly. These nonconvergence areas are reduced drastically when the retrieval of hydrometeor products is included, and the multiple scattering option is turned on in the forward model. The system convergence is modulated by computed instrument errors and by estimated modeling errors. The system is applied operationally to NOAA-18, NOAA-19, and Metop-A Advanced Microwave Sounding Unit (AMSU) and Microwave Humidity Sensor (MHS) sensors, as well as to DMSP-F16 (and soon F18) SSMI/S. It is also being applied routinely to Advanced Microwave Scanning Radiometer for Earth Observing System (EOS) (AMSR-E) and to National Polar-orbiting Operational Environmental Satellite System (NPOESS) Preparatory Project/Advanced Technology Microwave Sounder (NPP/ATMS) proxy data in preparation for the NPP launch that is scheduled in October 2011. The assumed modeling errors are around 1 K in all situations, except for

0196-2892/$26.00 © 2011 IEEE

This article has been accepted for inclusion in a future issue of this journal. Content is final as presented, with the exception of pagination.

the temperature-sounding channels, where they are estimated to be lower (between 0.17 K and 0.45 K depending on the channel). A suite of products, including atmospheric, surface, and hydrometeor parameters, is available on an operational basis from the MiRS algorithm, and it will be presented in this paper. In addition, the software package is also made available to the scientific community, and it could be obtained upon signing a *free-of-charge* licensing agreement. The system could also be an excellent tool to preprocess and filter microwave data for NWP assimilation applications based on the convergence metric and other parameters. The strictness of the filtering could easily be adjusted to fit users' needs. An additional benefit would be to provide an estimate of the geophysical state before starting the assimilation. This might be useful especially if there is an interest in assimilating measurements made in cloudy and rainy conditions and/or if there is interest in extending the assimilation over nonstandard surface backgrounds, such as coastal areas, sea ice edges, etc. Section II describes the MiRS scientific basis in detail. Section III gives an overview of the technical implementation of MiRS. It shows that MiRS is a full end-to-end processing system performing all the preprocessing and postprocessing functions, including footprint matching, bias correction, and interpretation of the primary products into derived products. Section IV presents the assessment of the quality of the MiRS products. This is an assessment done on a daily basis to make sure that there are no anomalies or significant drifts. It is performed using global NWP analyses and other sensor data products. It is different from the validation performed using a more highly valued ground reference data such as radiosondes, radar, and rain gauges. Note that the assessment presented here is a high-level overview of the performances in order to accompany the overall description of the MiRS system. In-depth analysis of the performances of specific parameters has been, or will be for some others, the object of dedicated studies published separately [4], [13], [16]. This paper concludes in Section V.

II. MIRS SCIENTIFIC BASIS

A. Overview of the Inversion Approach

MiRS is a 1-D variational (1DVAR) inversion scheme [2] that employs the CRTM [26] as the forward and AD operators. It solves for the surface and the atmospheric parameters simultaneously, including hydrometeors. The surface is represented by its temperature and emissivity spectrum. The atmosphere is represented by the temperature, moisture, nonprecipitating cloud, and rain profiles (in both liquid and frozen phases). Besides these primary parameters, other products are derived either by performing simple vertical integration [the case of the total precipitable water (TPW), cloud liquid water (CLW), ice water path (IWP), and rain water path (RWP)] or by performing a more elaborate postprocessing described later in Section III-F. This is the case of the surface rainfall rate (RR) based on the hydrometeor parameters, for example, or the snow and ice properties based on the emissivity vector.

B. MiRS Mathematical Basis

The iterative process of the 1DVAR inversion scheme employed in this paper aims at minimizing the following cost function, similar to the variational radiance data assimilation employed in NWP models:

$$J(X) = \left[\frac{1}{2}(X - X_0)^T \times B^{-1} \times (X - X_0)\right] + \left[\frac{1}{2}\left(Y^m - Y(X)\right)^T \times E^{-1} \times \left(Y^m - Y(X)\right)\right]$$

where X_0 and B are the mean vector (background) and error covariance matrix of X, which is the state vector to be retrieved, respectively. E is the measurement and/or modeling error covariance matrix. The first term on the right J_b represents the penalty in departing from the background value (*a priori* information), and the second right term J_r represents the penalty in departing from the measurements Y^m. Solving for this equation assumes that we have a forward operator Y that can simulate radiances similar to the measurements without bias and with statistics well captured within E. The solution that minimizes this two-term cost function is sometimes referred to as a constrained solution. The minimization of this cost function is also the basis for the variational analysis retrieval. The solution that minimizes this cost function is easily found by solving for

$$\frac{\partial J(X)}{\partial X} = 0$$

and by assuming a local linearity around X, which is generally a valid assumption if there is no discontinuity in the forward operator. This results in the following background-departure-based solution:

$$\Delta X_{n+1} = \left\{BK_n^T\left(K_nBK_n^T + E\right)^{-1}\right\} \times \left[(Y^m - Y(X_n)) + K_n\Delta X_n\right]$$

where n is the iteration index. K, in this case, is the Jacobian or the derivative of Y with respect to X.

At each iteration n, we compute the new optimal departure from the background, given the derivatives as well as the covariance matrices. This is an iterative numerical solution that accommodates moderately nonlinear problems and/or parameters with moderately non-Gaussian distributions. This approach to the solution is generally labeled under the general term of *physical* retrieval and is also employed in NWP assimilation schemes coupled with horizontal and temporal constraints (3DVAR and 4DVAR, respectively). As mentioned earlier, the entire geophysical vector is retrieved as one entity, including the temperature, moisture, and atmospheric hydrometeor profiles, as well as the skin surface temperature and emissivity vector, ensuring a consistent solution that fits the radiances. To address the ill-posed nature of the problem, the retrieval is performed in a reduced space. Empirical orthogonal functions (EOFs) are computed for the geophysical background covariance matrix B to diagonalize it. B is composed of atmospheric, hydrometeor, and surface components to account for (and benefit from) natural correlations that exist between these parameters. More details about the construction of this covariance will be given in Section III-D. The transformation matrix (eigenvectors) is then used to project back and forth between the original and

This article has been accepted for inclusion in a future issue of this journal. Content is final as presented, with the exception of pagination.

reduced spaces. It is important to note that the geophysical parameters of water vapor, cloud, rain, and ice are transformed into the logarithmic space before the retrieval. This is done for the twofold purpose of avoiding the negative values and making their distributions more Gaussian, which is a necessary condition for an optimal variational inversion.

C. First Guess

The first guess, distinct from the mean background in the MiRS algorithm, is used to start the iterative process. If the cost function has only one minimum, then the first guess would have, in theory, no impact on the result of the retrieval. However, it could help to speed up the convergence process if it is able to set the first estimate closer to the solution than the background itself. This is distinct from the mean background, which is a term in the formulation of the cost function, and therefore, it has a direct impact on the solution, which is the vector that minimizes the cost function. The background is derived from climatological data sets as described in the next section. The MiRS first guess is a multilinear regression algorithm, developed by collocating satellite measurements with NWP analyses and by establishing a relationship between the geophysical parameter that we want to regress and the sensor's brightness temperatures. Note that this relationship is done offline, and the resulting coefficients, distinct for each surface type and sensor, are used on the brightness temperatures obtained daily to generate first guess estimates for each individual observation. It is therefore important to highlight that there is no use of NWP forecast or analysis fields (even surface pressure) in the MiRS retrieval, either as the first guess or as the background.

D. Geophysical Background Covariance Matrix and Surface Classification

The geophysical background covariance matrix is used to constrain the state vector of the variational retrieval to within physically realistic solutions while maintaining consistency among the parameters and fitting the radiances. The covariances for all state vector parameters are generated using the European Centre for Medium-Range Weather Forecasts (ECMWF) 60 layer sample data set [5], ECMWF analyses [12], and model output fields from the Penn State/NCAR Mesoscale Model 5 [6], [10]. The geophysical background covariances represent the natural climate variability and cross-correlations for all parameters of the state vector and not the error of the background as is typical within NWP data assimilation systems.

The geophysical background covariance matrix in MiRS has three components. One covariance matrix is dedicated to atmospheric temperature and humidity. This matrix also contains the correlation with skin temperature to account for the natural linkage between lower-atmospheric and surface temperatures. The second covariance matrix is associated with cloud, ice, and rain hydrometeors. Note that this covariance is cross-correlated to the previous clear sky covariance to account for the natural linkages between the temperature and moisture and the presence of rain and/or ice in the atmosphere. An illustration of this composed atmospheric covariance matrix is shown in

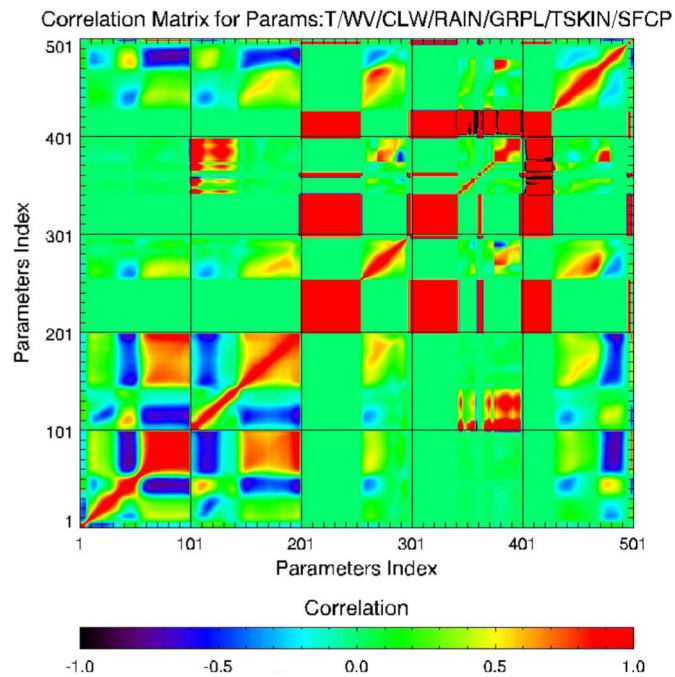

Fig. 1. Illustration of the covariance matrix used in MiRS for all parameters, including temperature sounding indexes [1–100], moisture sounding [101–200], nonprecipitation cloud profile [201–300], liquid rain profile [301–400], ice profile [401–500], skin temperature, and surface pressure (note that the covariances are, for illustrative purposes, shown as negative and positive correlations, which are a more meaningful way to look at covariances).

Fig. 1, with covariances represented as correlations since they allow a more straightforward interpretation. The exact formula used to compute these covariances is given in the following:

$$\sigma_{ij}^2 = \frac{1}{N}\sum_{i=1}^{N}\sum_{j=1}^{N}(x_i - \overline{x}_i) \times (x_j - \overline{x}_j)$$

where σ_{ij} is one of the elements of the matrix corresponding to row i and column j. N is the number of profiles used to compute the statistics, and $\overline{x}$ is the average value along the row or along the column. The correlations shown in the figure represent covariances normalized by the product of the corresponding variances.

The third covariance matrix is dedicated to surface emissivity. It contains several means and covariances which depend on the surface type. The emissivities for all surfaces are computed analytically using NWP data collocated with satellite radiances [14], [25]. The analytical emissivity is computed by assuming the following simplified radiative transfer equation:

$$T_B = \varepsilon \times T_s \times \Gamma + T^{\uparrow} + T^{\downarrow} \times (1 - \varepsilon) \times \Gamma$$

where T_B is the brightness temperature,ε is the emissivity that we would like to compute, T_s is the surface temperature, $T^{\uparrow}$ and $T^{\downarrow}$ are the upwelling and downwelling radiances, respectively, and Γ is the total atmospheric transmittance. Assuming that NWP analyses can provide accurate temperature and moisture profiles as well as a relatively accurate estimate of skin temperature, using the CRTM to compute the total transmittance, we can obtain the emissivity analytically by solving the previous equation for the emissivity value (sole unknown). This gives

This article has been accepted for inclusion in a future issue of this journal. Content is final as presented, with the exception of pagination.

us a relatively accurate estimate of the emissivity to compare to the one retrieved by the MiRS. The analytical emissivity is therefore computed using

$$\varepsilon = \frac{\left(\frac{T_B - T^{\uparrow}}{\Gamma} - T^{\downarrow}\right)}{T_s - T^{\downarrow}}.$$

The following four conditions need to be satisfied for this analytical emissivity to be valid: 1) $\Gamma \neq 0$ (the equation is not usable for opaque channels); 2) $T_s \neq T^{\downarrow}$ (the solution could be unstable if this condition is not satisfied); 3) the surface is assumed specular (for the validity of the simplified RT equation); and 4) the atmosphere is assumed as clear sky (no cloud, no rain, and no ice). The surface types included are ocean, land, snow, and sea ice. When performing retrievals on measurements, one of the first steps is to preclassify the surface spot corresponding to the measurements. Depending on the preclassifier, the specific mean and covariance matrix will be extracted from the master covariance matrix and will be used to constrain the amplitude and spectral shape of the emissivity spectrum. The emissivity vector is varied within the iterations based on the radiances and the CRTM Jacobians until a fit to the radiances is found. A postprocessing step is then undertaken to interpret the obtained emissivities into a set of derived products. These include the snow water equivalent (SWE), the sea ice concentration (SIC), and other snow and ice pack properties. A postprocessing surface type is also determined to reflect the retrieved emissivity spectrum. More details about the postprocessing are given in Section III-F.

E. Channel Usage

Recognizing that, for most microwave channels, there is a multitude of parameters that could have an impact on the measurements, we adopted the approach of using all channels together to retrieve all parameters simultaneously. This maximizes the information content available and accounts for the impacts from the multitude of parameters that affect the channels as much as possible, assuming that the sensor data is of high quality and that the RTM can simulate the measurements with low uncertainty. Lower-atmospheric temperature sounding channels, for instance, are sensitive to the surface, cloud, and tropospheric humidity. Water vapor sounding channels also have nonnegligible sensitivity to temperature, ice, cloud, and rain. Surface-sensitive channels are also sensitive to the presence of cloud, rain, and water vapor. Therefore, this approach is adopted in MiRS to solve for all parameters simultaneously to benefit from their sensitivity to multiple channels and intercorrelations. Another important reason is that the obtained solution must fit all of the radiances measured simultaneously. This is often an overlooked condition that must be satisfied. Alone, it is not a sufficient condition to obtain the right solution, but it is a necessary one. What is meant by this is shown in Fig. 2. What we can say with certainty is that, if the state vector retrieved is not satisfying the condition of fitting all measurements at the same time, the retrieval is not the solution (otherwise, the measurements are assumed wrong). Fitting the measurements

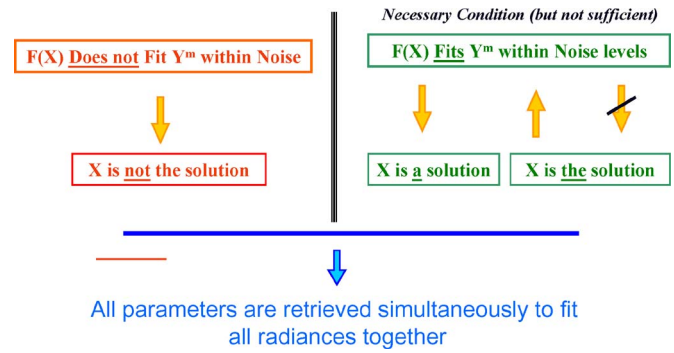

Fig. 2. Illustration of the necessary condition of having the retrieved solution fit all measurements simultaneously.

is, on the other hand, only a necessary condition to obtain a solution within the domain of possible solutions.

In theory, this should advocate for the usage of a simultaneous and comprehensive approach to the retrieval of geophysical parameters and, as a corollary, should discourage the usage of independent single-parameter retrieval algorithms which have no mechanism to ensure that the obtained products will satisfy this condition of fitting all measurements simultaneously.

F. Radiative Transfer and Jacobians

This inversion of cloudy/rainy radiances supposes the use of a forward operator that can simulate the multiple scattering effects due to ice, rain, snow, graupel, and CLW at all microwave frequencies and that can generate the corresponding Jacobians for all atmospheric and surface parameters. As mentioned earlier, the forward operator used in this paper is the CRTM developed at the Joint Center for Satellite Data Assimilation (JCSDA). CRTM produces radiances, as well as Jacobians, for all geophysical parameters. It is valid in clear, cloudy, and precipitating conditions. Derivatives are computed using the k-matrix developed by TL and AD approaches. This is ideal for retrieval and assimilation purposes. The different components of CRTM, briefly, are the OPTRAN fast atmospheric absorption model [21], the National Environmental Satellite, Data, and Information Service (NESDIS) microwave emissivity model [26], and the advanced doubling-adding radiative transfer solution for the multiple scattering modeling [18]. Note that CRTM is also the official radiative transfer model employed at the National Centers for Environmental Prediction (NCEP), National Oceanic and Atmospheric Administration (NOAA). Also, note that MiRS is, in theory, valid for all sensors for which CRTM is valid, although it has been applied and assessed (in this paper) for microwave sensors only.

G. EOF Decomposition

The retrieval in MiRS is performed in EOF space through projections back and forth at every iteration between the original geophysical and reduced spaces. With the limited number of microwave channels available through operational sensors, the projection of the observations into the EOF space is not applied. This method has been routinely used in operational centers as a standard transform approach of control variables [19]. It

This article has been accepted for inclusion in a future issue of this journal. Content is final as presented, with the exception of pagination.

has also been used in the context of retrieval of trace gases, sounding, and surface properties [18], [23], [24]. Applying it in the context of our 1DVAR retrieval is therefore not very original except, possibly, for its extension to cloudy and precipitating profiles. Only a limited number of eigenvectors/eigenvalues are kept in this reduced space. The selection of how many EOFs to use for each parameter is somehow subjective, but it depends on the number of channels available that are sensitive to that parameter. The advantages of performing the retrieval in EOF space are the following: 1) handling the strong natural correlations that sometimes exist between parameters which usually create a potential for instability (or oscillation) in the retrieval process (small pivot), which is reduced significantly by performing the retrieval in an orthogonal space, and 2) time saving by manipulating and inverting smaller matrices. The projection in EOF space is performed by diagonalizing the *a priori* covariance matrix

$$B \times L = L \times \Theta$$

where L is the eigenvector matrix, also called as the transformation matrix, and Θ is the eigenvalue diagonal matrix which contains the *independent* pieces of information. The retrieval is therefore performed using the matrices/vectors Θ, $\overline{\Delta X}$, and $\overline{K_n}$ (retrieval in reduced space). The transformations back and forth between the two spaces are done using the transformation matrix L. It is important to note that, at this level, no errors are introduced into these transformations; it is merely a matrix manipulation. However, the advantage of using the EOF space is that the diagonalized covariance matrix and its corresponding transformation matrix can be truncated to keep only the most informative eigenvalues/eigenvectors. By doing so, we are bound to retrieve only the most significant features of the profile while leaving out the fine structures. How much truncation depends on how much information is contained in the channels. In the AMSU configuration, eight EOFs are used for temperature, four for humidity and surface emissivity, one for skin temperature, three for nonprecipitating cloud, and three for both rain and frozen precipitation (a total of 20 nonprecipitating conditions and a total of 22 precipitating conditions). It should be noted that the same constraints are used for temperature and water vapor retrievals regardless of precipitating or nonprecipitating scenes.

III. MIRS SYSTEM IMPLEMENTATION

The previous section presented the general approach of MiRS, the scientific options adopted, and the rationale behind them. In this section, we will present the technical details of the implementation which are important to understand. It also touches on the issue of the convergence, which is significant for two reasons: it determines if the essential condition for finding a solution is met, and it plays the role of a powerful quality-control metric.

A. Overview of the MiRS System

Fig. 3 shows how the MiRS works at a general level. There are, in fact, two loops within the MiRS. In the first attempt retrieval, the system assumes a rain-free and ice-free atmosphere, disabling the multiple scattering feature and assuming pure absorption from nonprecipitating cloud. This first attempt generally reaches convergence roughly 90%–95% of the time. In case a convergence is reached, as shown in Fig. 3, then the system exits with a valid output (but with no rain or ice by definition). For the remaining 5%–10%, the cause of nonconvergence could be due to certain factors such as mischaracterization of the surface properties, overly strict convergence criteria, or the inability of the RTM to account for some phenomena. With MiRS, the latter is assumed specifically because the multiple scattering is not activated during the first retrieval attempt and because the RTM has the inability to model the signal caused by the precipitation or frozen hydrometeors. Therefore, in the second retrieval attempt, multiple scattering is turned on. In this case, no nonprecipitating cloud is retrieved, given the radiometric difficulty in distinguishing what is precipitating and what is suspended liquid water. The EOF distribution is also altered slightly in this second attempt, as noted in the previous section.

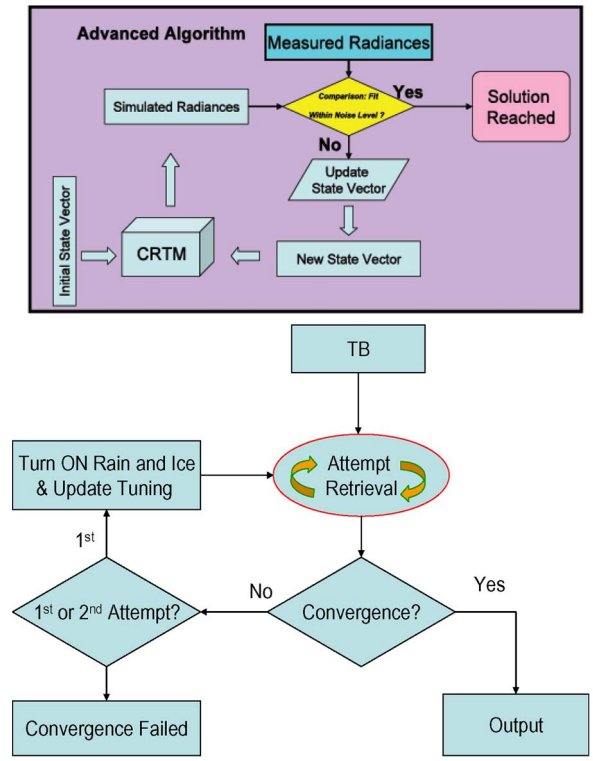

Fig. 3. Diagrams of the MiRS retrieval algorithm. The bottom panel describes the retrieval attempts. The top panel shows the iterative approach adopted in MiRS to reach a solution within each retrieval attempt. See text for details.

For each retrieval attempt, the iteration loop is the same, and it is also shown in Fig. 3. To start the iteration process, an initial state vector is used as the input to the CRTM forward model, and it is assumed to be the first guess estimate. During the iterative process, the state vector is altered using the process described in Section II-B. This vector is deemed to be the solution when the measurements are fit to within noise and RTM uncertainty, and convergence has been reached.

This article has been accepted for inclusion in a future issue of this journal. Content is final as presented, with the exception of pagination.

TABLE I
OVERVIEW OF OPERATIONAL PRODUCTS FROM MiRS. THE SENSORS ARE NOAA-18/19, METOP-A, AND DMSP-F16 SSMI/S

Versions	Scheduled Deliverables	Operational Status
MIRS v1.0	Temperature Profiles over ocean (N18 & MetOp-A) Moisture Profiles over ocean (N18 & MetOp-A) Total Precipitable Water (TPW) over ocean (N18 & MetOp-A) Land Surface Temperature (N18 & MetOp-A) Emissivity Spectrum over land and snow (N18 & MetOp-A)	August 30, 2007
MIRS v2.0	**Enhanced v1.0 products plus:** Extension of Moisture Profiles over non-costal land (N18 & MetOp-A) Extension of TPW over non-costal land (N18 & MetOp-A) Extension of emissivity spectrum over all surface (N18 & MetOp-A) Snow Water Equivalent over land (N18 & MetOp-A) Snow Cover over land (N18 & MetOp-A) Sea-Ice Concentration over ocean (N18 & MetOp-A) Cloud Liquid Water over ocean (N18 & MetOp-A)	March 30, 2008
MIRS v3.0	**Enhanced v2.0 products plus:** Ice Water Path (N18 & MetOp-A) Rain Water Path (N18 & MetOp-A) TPW over ocean and non-costal land (SSMIS) Surface Temperature over land (SSMIS) Emissivity Spectrum over all surfaces (SSMIS)	October 27, 2008
MIRS v4.0	**Enhanced v3.0 products plus:** Rain Rate (N18 & MetOp-A) Snow Water Equivalent over land (SSMIS) Snow Cover over land (SSMIS) Sea-Ice Concentration over ocean (SSMIS) Cloud Liquid Water over ocean (SSMIS)	March 31, 2009

B. MiRS Capability and Operational Implementation

The MiRS system was implemented operationally in several phases, allowing a gradual increase in capabilities in terms of the number of products and the number of sensors supported. Table I describes the timeline of the MiRS operational implementation and, for each phase, lists the sensors, as well as the products, it declared operational. In addition to these operational products, demonstration products are also available without being declared officially operational: sea ice type (multiyear and first year), snow effective grain size, and temperature and moisture profiles for DMSP-F16 SSMI/S. The most recent version (5.0) at the end of 2009 extended SSMI/S products to include the RWP, IWP, and RR.

C. Noise Estimation

Whenever possible, i.e., when having access to original radiometric counts, such as in the case of AMSU and MHS onboard NOAA-18/19 and Metop-A, MiRS computes an accurate instrument noise estimate, following the approach described in [22]. This is based on the standard deviation of the differences between the radiometrically computed and measured temperatures of the hot calibration load. When access to these counts is not possible, MiRS relies on advertised values of instrument noise levels for those particular sensors (such as SSMI/S).

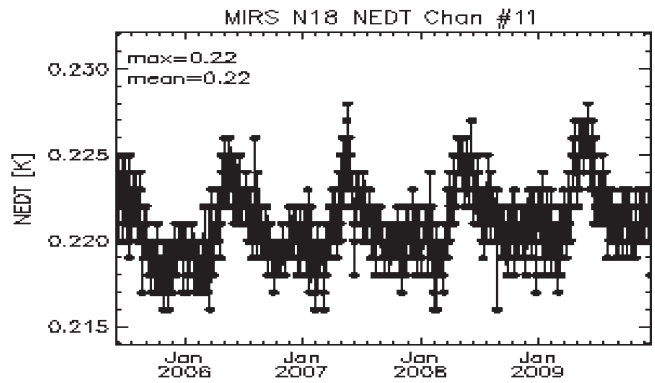

Fig. 4. Time series of the noise level for channel #11 of AMSU (57 GHz) onboard NOAA-18 since its launch time in mid-2005. This channel is aimed at sounding temperature. Slight seasonal variations are noticed, with no expected impact on the retrievals.

This noise estimate (NeDT), when computed, is monitored on a daily basis to detect any anomalies or drifts. This noise is an input to the 1DVAR algorithm. This has the effect of automatically reducing the weight of a particular channel in the solution-finding process when the instrument's noise level increases.

An illustration of the noise level monitoring for NOAA-18 since its launch in mid-2005 is shown in Fig. 4. If the computed noise exceeds the expected range of variation (defined by instrument specifications), an electronic mail notification is triggered.

This instrument noise represents the first part in matrix E presented in Section II-B. The other part represents the radiative transfer model uncertainty, which will be described in more detail in Section III-E.

D. Footprint Matching

AMSU/MHS and SSMI/S sensors have their individual channels looking at slightly different horizontal footprints on the Earth in terms of size. The footprint size for AMSU is 45 km at nadir, while MHS is 15 km. Because a 1DVAR system is computationally more demanding than regression-based algorithms, MiRS runs operationally at AMSU resolution for the case of NOAA-18, NOAA-19, and Metop-A, where MHS footprints are simply averaged within the AMSU footprint, as shown in Fig. 5. There are plans, however, to start running MiRS at a higher resolution in the near future (MHS resolution).

For the case of SSMI/S, for pure computation time constraints, all channels [environmental channels (ENV), imaging channels (IMG), and lower atmospheric sounding channels (LAS)] are mapped by a simple averaging to the upper atmospheric sounding (UAS) channel resolution. The MiRS resolution, when run on SSMI/S data, is therefore that of UAS channels, which is approximately 75 km for all scan positions. The resolutions for IMG, ENV, and LAS channels are 12.5, 25, and 37.5 km, respectively (Fig. 6).

E. Bias Correction and RTM Uncertainties

The radiances, before being ingested into the MiRS algorithm, are bias corrected. This correction removes potential

This article has been accepted for inclusion in a future issue of this journal. Content is final as presented, with the exception of pagination.

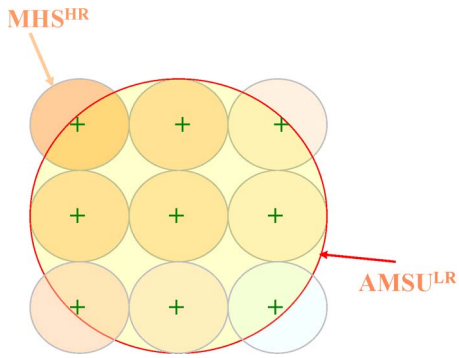

Fig. 5. Schematic description of the scan geometry and the footprint matching performed for the AMSU/MHS sensor pair onboard (NOAA-18, NOAA-19, and Metop-A). The single AMSU footprint is depicted by the larger circle, which encompasses the MHS footprints depicted by the nine smaller circles.

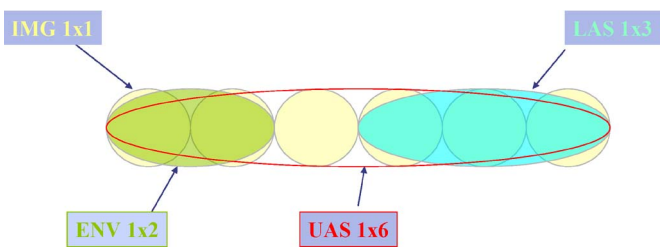

Fig. 6. Schematic description of the scan geometry and the footprint matching performed for the SSMI/S sensor onboard DMSP-F16. The largest circle represents the UAS footprint, with 1×1, 1×2, and 1×3 circles representing the IMG, ENV, and LAS footprints, respectively.

inconsistencies between the measurements and the forward model used in MiRS. A set of different coefficients is generated offline for every sensor. The coefficients are also generated for different scan positions (or angles for the case of cross-track sensors) to account for any scan asymmetry anomalies. The approach used to compute these biases relies on comparisons between simulations and measurements of brightness temperatures. The simulated radiances in this case use the CRTM forward model and take ECMWF from multiple seasons as inputs, interpolated in time and space to the specific locations of the measurements. These comparisons are done exclusively over the ocean because the emissivity over nonocean surfaces is not known, which limits the possibility to determine biases for surface-sensitive channels. Over the ocean, we use surface wind speed as an input to the emissivity model FASTEM-3 [7] to generate emissivities. These emissivities, combined with atmospheric parameters from the analyses, allow the generation of the simulated brightness temperatures which are then compared to real measurements. In addition to biases, the comparisons are also used to generate estimates of radiative transfer model (RTM) uncertainties which help in making up the instrument/modeling error covariance matrix E when combined with instrument noise estimates. These RTM uncertainties are calculated via the standard deviation of the radiance comparisons, scaled down to account for uncertainties in the geophysical inputs themselves. The specific RTM uncertainties for AMSU-A, MHS, and SSMI/S channels are captured in Table II.

It is well known that the radiance corrections are highly affected by cloud and coastal contamination, even if we limit ourselves to nominal ocean cases. The issue of bias, or more explicitly how to handle the inconsistencies between the measurements and the RTM used in the retrieval algorithm, could be the subject of a study by itself given its complexity. Methods to remove these biases range from calculating a statistical bias to using quantities of geophysical parameters as predictors to estimate the bias for a given scene depending on its air mass properties. Regardless of the approach, care should be taken to choose the appropriate scenes for calculating biases without contamination or introduction of artifacts, such as seasonal dependence. For the purpose of this paper, we have made the choice of computing the corrections by adjusting the peak of the histograms of the error distributions for all channels and all scan positions to coincide with zero. This has the advantage of reducing the dependence of the obtained correction on cloud filtering, coastal scene removal, etc. These less frequent contaminations tend to materialize in the tail end of the error distributions which are Gaussian, to which the peak of the histogram is usually insensitive.

Note that, for the case of DMSP-F16 SSMI/S data, it is known that these display obvious radiance anomalies due to the main antenna emission and the solar intrusion to warm load [1], [17], [28]. The SSMI/S data used in this paper are the anomaly corrected data.

F. VIPP

The postprocessing stage in MiRS mentioned earlier is shown in Fig. 7. After the 1DVAR step is performed, a number of primary products are generated. These are the surface, atmospheric, cloud, and hydrometeor parameters that most directly impact the brightness temperatures. These core products are then *translated* into derived products via two mechanisms. The first one is vertical integration, and the second one is postprocessing.

1) Vertical Integration: The retrieved moisture profile is vertically integrated to generate the TPW, which, by definition, ensures there is consistency between the profile and the TPW (as opposed to retrieving the TPW as a separate product). A similar vertical integration is performed to generate RWP, IWP, and CLW, as shown in Fig. 7. One word of caution is warranted when mentioning CLW, IWP, and RWP. These parameters impact the brightness temperatures and have some signal in the measurements, but it is critical to keep in mind that their impact is mixed with that of the size of the droplets, the vertical distribution, the particle size distribution, the density, the mixed phase nature, and the shape of the droplets. The problem is therefore notoriously ill-constrained. In addition, the beam filling effect, the uncertainty in the modeling of the scattering, the absorption, the asymmetry and their temperature dependence, and the resulting products become essentially *effective* parameters that account for all of these unknowns. These products are therefore destined for what we label as *advanced* users who realize that the absolute amounts of CLW, IWP, and RWP need to be used with care, given that they depend significantly on the assumptions made about those unknowns mentioned previously (especially the droplet mean sizes). For example, alternate assumptions about rain drop particle size

This article has been accepted for inclusion in a future issue of this journal. Content is final as presented, with the exception of pagination.

TABLE II
INSTRUMENT MODELING ERROR FOR AMSU-A AND MHS CHANNELS FOR MiRS APPLIED TO NOAA-18, NOAA-19, AND METOP-A (M2) AND FOR SSMI/S CHANNELS FOR MiRS APPLIED TO F16 AND F18

AMSU-A/MHS				SSMI/S		
	N18	N19	M2		F16	F18
Frequency (GHz)	Error (K)	Error (K)	Error (K)	Frequency (GHZ)	Error (K)	Error (K)
1. 23.8	0.69	0.69	0.79	1. 50.3*	0.90	1.40
2. 31.4	0.58	0.58	0.59	2. 52.8*	0.75	0.91
3. 50.3	0.38	0.38	0.43	3. 53.6*	0.43	0.47
4. 52.8	0.34	0.34	0.42	4. 54.4*	0.28	0.22
5. 53.6	0.26	0.26	0.24	5. 55.5*	0.37	0.34
6. 54.4	0.16	0.16	0.15	6. 57.2	0.41	0.38
7. 54.9	0.22	0.22	0.21	7. 59.4	0.39	0.31
8. 55.5	0.23	0.23	0.21	8. 150.0	3.23	2.78
9. 57.2 (1)	0.21	0.21	0.21	9. 183.3 ± 6.6	1.55	1.75
10. 57.2 (2)	0.21	0.21	0.22	10. 183.3 ± 3	1.32	1.50
11. 57.2 (3)	0.24	0.24	0.25	11. 183.3 ± 1	1.37	1.30
12. 57.2 (4)	0.34	0.34	0.36	12. 19.3 H	2.20	1.81
13. 57.2 (5)	0.59	0.59	0.62	13. 19.3 V	1.61	1.34
14. 57.2 (6)	1.25	1.25	1.27	14. 22.2 V	1.67	1.37
15. 89.0	0.96	0.96	1.11	15. 37.0 H	3.34	2.16
16. 89.0	1.00	1.00	1.16	16. 37.0 V	2.32	1.58
17. 157.0	0.82	0.82	1.08	17. 91.6 H	1.48	1.43
18. 183.3 ± 1	1.02	1.02	0.99	18. 91.6 V	2.64	2.44
19. 183.3 ± 3	0.94	0.94	0.93	19-24. (60.7-63.2 GHz) are not modeled.		
20. 190.3	1.04	1.04	1.05			

* F16 Channels 1-5 are Vertical Polarization. F18 Channels 1-5 are Horizontal Polarization.

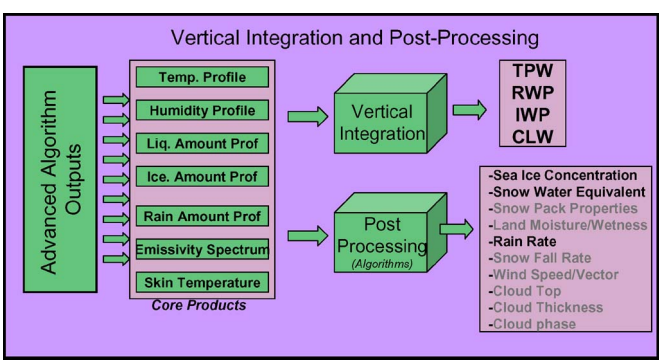

Fig. 7. Description of the MiRS postprocessing stage. See text for more details. The operational products generated by the VIPP include TPW, IWP, RWP, CLW, SIC, SWE, and RR. Other products could be generated in future versions of MiRS (wind speed/vector, cloud top, thickness, phase, and snowfall rate).

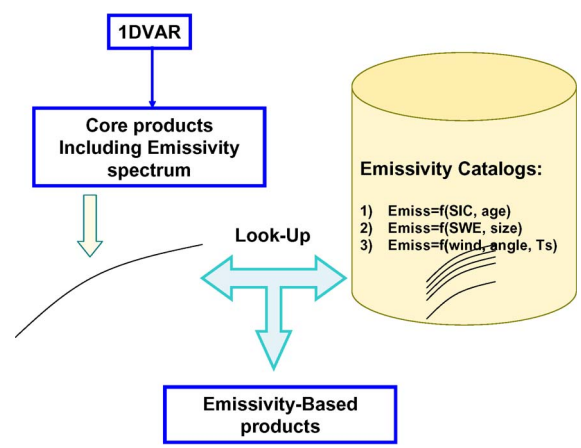

Fig. 8. Details of the postprocessing stage of MiRS that deals with the interpretation of the retrieved emissivity spectrum. See text for further details.

distributions could yield different RWP retrieval results given the same set of observations. These assumptions are made, in the case of MiRS, inside the forward operator CRTM. If enough information was available within the radiometric measurements themselves, these unknowns could be included within the retrieved state vector. This is not the case with the limited number of channels available in the current microwave sensors.

2) Emissivity Postprocessing: The second type of postprocessing, shown in Fig. 8, is the interpretation of the emissivity spectrum (spectra are represented schematically by multiple curves in the figure). Recall that the emissivity is made part of the retrieved state vector to simplify the overall retrieval and to solve for the parameters that most directly impact the brightness

This article has been accepted for inclusion in a future issue of this journal. Content is final as presented, with the exception of pagination.

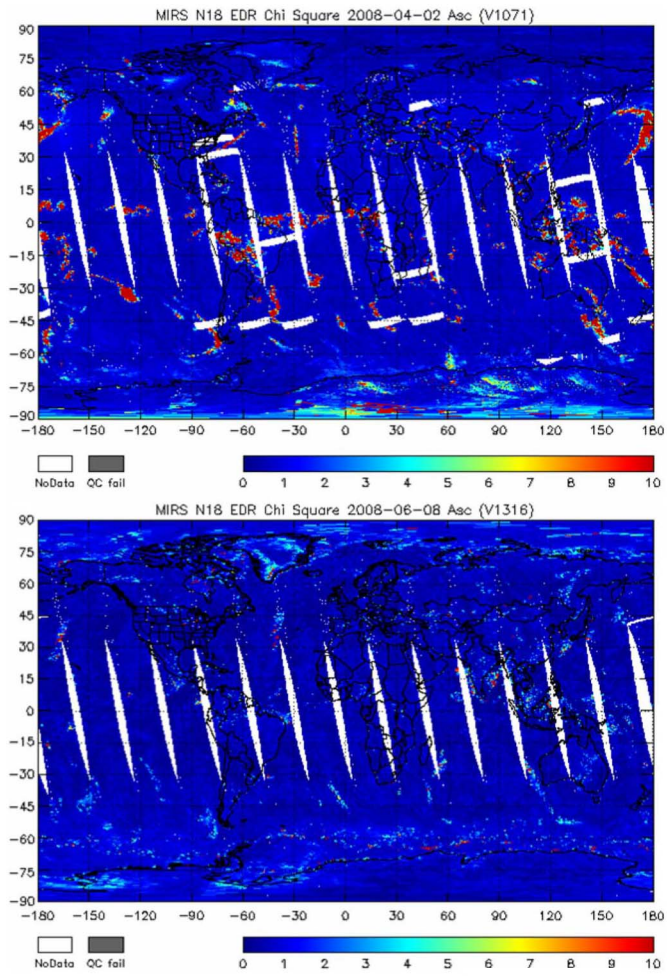

Fig. 9. Comparison of the convergence metrics between two versions of the MiRS, (top) with the multiple scattering turned off and (bottom) with the multiple scattering on. Convergence, as defined in the text, is reached almost everywhere, including when there is precipitation.

temperatures first. Although the emissivity could be used by itself (for instance, as a proxy parameter for the degree of wetness over land), it is also desirable to interpret the magnitude and shape of the retrieved emissivity spectrum into more readily usable products. SIC over sea ice and SWE over snow-covered land are currently derived from the emissivity spectrum using a postprocessing step.

This interpretation of the emissivity spectrum relies on the development of an offline-computed catalog of emissivity spectra for a multitude of values of the parameters to be derived. The postprocessing stage is then a simple look-up-table procedure that searches for the catalog precomputed value that corresponds to a spectrum that matches closely with the retrieved one. Along with the search of SIC, the type/age of the ice (multiyear and first year) is also cataloged and searched, given its importance/impact on the emissivity spectrum. Similarly, along with the search of SWE, the effective grain size is also cataloged and searched. These two by-products (sea ice type and effective grain size) are made available within MiRS products for testing purposes and are not officially declared operational.

3) Rain Rate Postprocessing: One important parameter retrieved by MiRS using vertical integration and postprocessing (VIPP) is the surface RR, which is discussed and analyzed at length in [13]. The importance of the RR is related to its direct societal impact. From the radiometric point of view, the more appropriate parameter is the instantaneous integrated rain amount in the vertical column at the time it is sensed, which has a direct impact on the brightness temperature measurement. Because the RR needs a time variability dimension to obtain the rate in millimeters per hour and because the sensors being considered use polar-based orbits (and not geostationary), we adopted an empirical relationship for deriving this parameter. The RR is retrieved using the rain, ice, and cloud profiles. It also uses the atmospheric temperature-based freezing level and the lower atmospheric temperature lapse rate, given their correlations with the presence or absence of the rain at the surface. This statistical relationship is generated using a number of runs of the cloud resolving model MM5. It is given generically in the following equation:

$$RR = A_0 + A_1 \times IWP + A_2 \times RWP + A_3 \times CLW$$

where the coefficients A_i, $i = 0, 1, \ldots$, are computed offline to capture the physical link between the hydrometeor parameters from the MiRS first step and the surface RR. It is important to note that the former is not sensor-specific parameters and that the relationship will apply for all sensors. Thus, one of the advantages of the MiRS RR retrieval is that it merely depends on a relationship which associates the RR presence and intensity with the combination of hydrometeors and geophysical products derived by the MiRS first step. The quality of the RR derived by this relationship will obviously be modulated by the quality of the inputs listed in the aforementioned equation. This latter quality depends on the information content in the measurements of the sensor being considered.

The assessment of the quality of the MiRS RR will be discussed later in this paper and will also be the object of a separate more detailed publication.

G. Convergence Criteria

Several criteria have been reported in deciding on the convergence of variational methods, among which are the following: 1) testing that the increment of the parameter values at a given iteration is less than a certain threshold (usually a fraction of the associated error of that particular parameter); 2) testing that the cost function $J(X)$ decrease is less than a preset threshold; or 3) checking that the obtained geophysical vector X at a given iteration produces radiances that fit the measurements within the noise level impacting the radiances. We have chosen the last criterion because it maximizes the radiance signal extraction. A convergence criterion based on $J(X)$, while mathematically correct, would produce an output that carries more ties to the background, and therefore, it would be more inclined to present artifacts due to it. The convergence criterion adopted is when

$$\varphi^2 = \frac{1}{N}\left[(Y^m - Y(X))^T \times E^{-1} \times (Y^m - Y(X))\right] \leq 1$$

where N is the number of channels used for the retrieval process. This mathematically means that the convergence is declared reached if the residuals between the measurements and

This article has been accepted for inclusion in a future issue of this journal. Content is final as presented, with the exception of pagination.

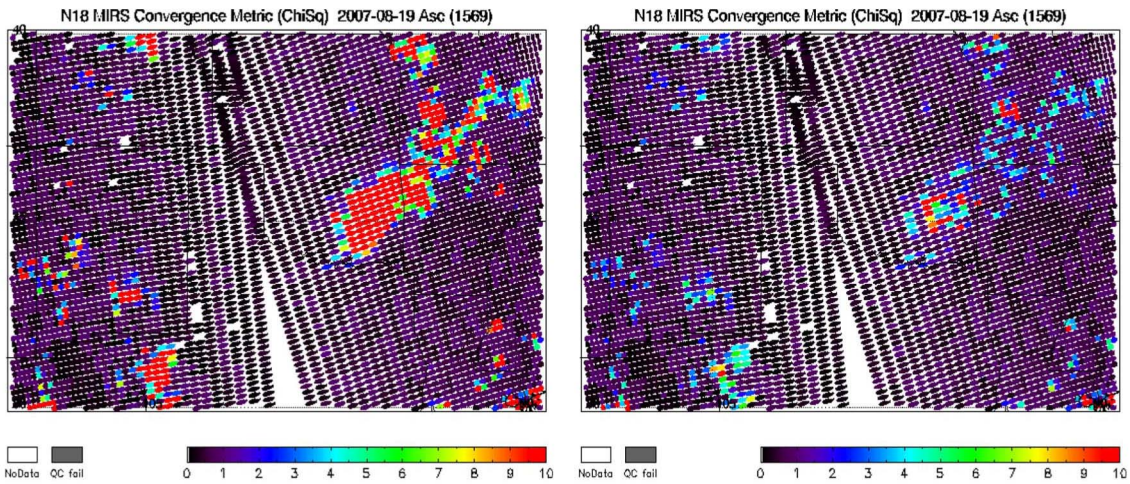

Fig. 10. Example of the convergence reached with MiRS over a tropical storm after the multiple scattering feature was turned on (right) during the retrieval. Although the convergence is much improved, there are pockets where the retrieval does not converge.

the simulations at any given iteration are less or equal than one standard deviation of the noise that is assumed in the radiances. Fig. 9 shows an example of daily maps of the convergence metric φ^2 as generated from MiRS.

This figure illustrates that the convergence is reached globally, with the φ^2 being close to unity in most cases (bottom panel). It also illustrates that including the multiple scattering option and solving for liquid and frozen hydrometeors in the state vector are key to achieving convergence in precipitating/icy conditions. This could be viewed as a highly nonlinear way of doing a *precip-clearing* of the radiances. The inclusion of these control parameters within MiRS allows, indeed, the retrieval to reach convergence and to produce other parameters such as the temperature profile. Note that the convergence map in Fig. 9, because of its size, hides some local nonconvergence in rainy conditions. Indeed, not every single point reaches convergence, as shown in Fig. 10 for a particular storm case. The nonconvergence will, however, be an indication of an abnormality in the retrieval: some difficult to model features, some mixed signal in the measurement (at the coast or sea ice edge for instance) for which a radiometric effective emissivity could not be found, etc. These cases could therefore easily be screened out using a filter based on the φ^2 parameter.

Note that fitting the radiances within the noise level is a necessary, but not a sufficient, condition in finding the right solution, as explained earlier. We should note here that the convergence criteria do not alter the balance of weights given to the radiances (or to the background) in the cost function that the 1DVAR minimizes.

H. MiRS Applicability to Extreme Weather Events

MiRS uses the CRTM for the generation of the simulated radiances and the Jacobians, which are both necessary for the successful variational retrieval. CRTM is valid in clear, cloudy, and rainy conditions, which makes MiRS also valid in those conditions. When we say valid, we mean that the convergence is reached, and a radiometric solution is found. This makes MiRS an ideal algorithm in inverting radiances measured in storm or hurricane conditions. As clearly shown previously in Fig. 9, the inclusion of hydrometeors in the retrieval and the use of a full multiple scattering radiative transfer allow us to reach the convergence globally. Fig. 10 shows a close-up of a retrieval field over a storm over the Continental United States (CONUS) before and after turning on the multiple scattering and including the liquid and frozen precipitations in the state vector. It shows that the convergence is dramatically improved, but a few points remain for which convergence was not obtained.

The solution, whose accuracy depends on many unknowns that cannot be determined because of the lack of information content, is constrained by the covariance matrix (and the cross-correlations between the different parameters that are contained in it), by the physically based Jacobians that indicate how the solution should be altered in order to fit the measurements, and by the physically based retrieval that fits the simulated radiances based on the solution to the radiances measured.

Obtaining convergence in extreme weather conditions, despite the physical constraints put on the solution, is not synonymous with accurate retrievals. From offline simulations (not shown here) where the true solution was known, it was concluded that the hydrometeor parameters and the temperature profile could be considered sufficiently accurate. On the other hand, the moisture profile, CLW, TPW, land surface temperature (LST), or emissivity is not to be used in the presence of atmospheric rain or ice. It is intuitively easy to understand that, with the presence of precipitating rain in the column, it is radiometrically difficult to distinguish the impact of the liquid water from the impact of the water in vapor form or from the nonprecipitating liquid water. If the rain is present in large enough quantity, it is also understandable that the signal from the surface will be screened out, thus reducing the capacity to retrieve surface parameters.

IV. MIRS ASSESSMENT

In this section, we will focus on presenting an overview of the assessment of the quality of the MiRS products. Because

This article has been accepted for inclusion in a future issue of this journal. Content is final as presented, with the exception of pagination.

TABLE III
OVERVIEW OF THE ASSESSMENT SOURCES USED FOR THE DIFFERENT MiRS PRODUCTS. NOTE THAT SOME OF THESE VALIDATIONS ARE PERFORMED DAILY (CUMULATING EVERY DAY) FOR THE FOLLOWING SENSORS: NOAA-18 AMSU/MHS, NOAA-19, METOP-A, AND DMSP-F16 SSMI/S. SEE TEXT FOR MORE DETAILS

EDRs	Ground Truth Sources used for Validation
Temp. profile	(1) Operational radiosondes, (2) Climate-quality radiosondes, (3) field campaigns acquired radiosondes, (4) GPS sounding, (5) GDAS, (6) ECMWF, (7) GFS fields, (8) GOES soundings, (9) dropsondes, (10) inter-consistency between sensors, (11) ATOVS heritage algorithm
Moist. profile	(1) Operational radiosondes, (2) Climate-quality radiosondes, (3) field campaigns acquired radiosondes, (4) GPS sounding, (5) GDAS, (6) ECMWF, (7) GFS fields, (8) GOES soundings, (9) dropsondes, (10) inter-consistency between sensors , (11) ATOVS heritage algorithm
Total precipitable water[1]	(1) Operational radiosondes, (2) Climate-quality radiosondes, (3) field campaigns acquired radiosondes, (4) GDAS, (5) ECMWF, (6) GFS fields, (7) GOES soundings, (8) dropsondes, (9) MSPPS heritage algorithm
Precip rate[1]	(1) Rain gauges, (2) CPC analyses, (3) IPWG, (4) radar data, (5) TRMM/TMI, (6) TRMM/PR, (7) MSPPS heritage algorithm, (8) FNMOC RR product (for SSMIS only)
Snow cover[1]	(1) MSPPS heritage algorithm, (2) FNMOC product (for SSMIS), (3) NASA AMSR-E product, (4) IMS (Interactive Multisensor Snow and ice Mapping System)
Snow water equivalent[1]	(1) MSPSP heritage algorithm, (2) FNMOC product (for SSMIS), (3) NASA AMSR-E product, (4) IMS (Interactive Multisensor Snow and ice Mapping System)
Sea ice concentration[1]	(1) MSPSP heritage algorithm, (2) FNMOC product (for SSMIS), (3) NASA AMSR-E products (bootstrap and team-2), (4) IMS (Interactive Multisensor Snow and ice Mapping System)
Cloud water[1]	(1) MSPPS heritage algorithm, (2) CLOUDSAT, (3) ECMWF
Ice water path[1]	(1) MSPPS heritage algorithm, (2) CLOUDSAT
Land temp[1]	(1) GDAS, (2) ECMWF, (3) HIRS
Land emis[1]	(1) GDAS-based wind-induced emissivity (over ocean), (2) ECMWF-based wind-induced emissivity (over ocean), (3) analytical emissivity using GDAS –over snow, sea-ice, land-, (4) analytical emissivities using ECMWF –over snow, sea-ice, land-
Hydr. Profile[2]	Qualitative assessment using TRMM (on-going)
Sea Surface Temperature[3]	(1), GDAS analyses, (2) ECMWF analyses
Snow & Ice Temperature[3]	(1), GDAS analyses, (2) ECMWF analyses

of the large number of products and because the scope of this paper is mainly the description of the MiRS system, the assessment presented here will be succinct but detailed enough to give confidence in the usage of these products. Additional publications dedicated to individual parameters will present thorough assessments of each product.

There are three types of assessments performed on MiRS-based products. 1) The first one is the routine assessment of the MiRS algorithm with respect to other algorithms, to NWP analysis, or to other sensors. This assessment generally offers a global coverage of the comparisons, as well as robust statistics, given the abundance of points. Stratification of the performances (by angle, by scan position, by latitude, etc.) is also made possible in this type of assessment. 2) The second type of assessment uses highly valued references to assess the performances and is the closest to the process of validation. Although the main advantage is the use of high-quality data (such as radar and gauge data for the RR assessment and radiosondes or dropsondes for the temperature and moisture profile assessment), it generally suffers from other limitations such as the geographical distribution of the reference data sources, the intravariablity of the reference data quality, and the representativeness of the footprint cell (w.r.t. the point measurement of the reference source). 3) The third type of assessment is simply a qualitative assessment of the behavior of MiRS products. The objective in this case is to ensure that the products behave individually and collectively in a physically and meteorologically consistent fashion. Table III lists all of the references used to assess MiRS products for each product.

A. Routine Assessment of MiRS Products

Routine assessment is done for all products of MiRS and for all sensors (NOAA-18, NOAA-19, Metop-A, and DMSP-F16 SSMI/S) using daily comparisons with NWP analyses from NCEP and ECMWF.

1) Temperature Sounding: Fig. 11 shows an example of that assessment in the form of maps of atmospheric temperature at 100 mbar, as inverted by the MiRS algorithm and as provided by *Global Data Assimilation System* (GDAS) analyses. Note that NWP analyses are interpolated in time and space to the exact location and time of the satellite measurement before this comparison is performed. We can see that all major features of the temperature field are well captured by MiRS retrievals. In Fig. 12, the same set of temperature profiles from MiRS and GDAS was used to compute vertical statistics of bias and standard deviation of the differences. Only cases over the ocean (which are officially declared operational) were used

This article has been accepted for inclusion in a future issue of this journal. Content is final as presented, with the exception of pagination.

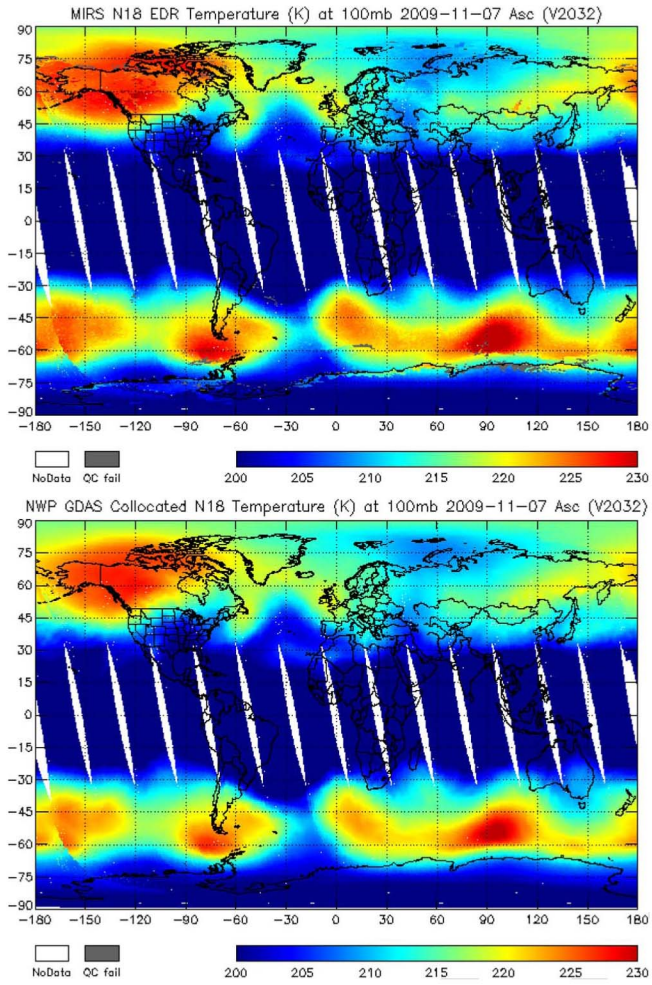

Fig. 11. Global fields of atmospheric temperature at the 100-mbar layer (top) as determined by the MiRS algorithm and (bottom) as provided by the GDAS analysis. Field corresponds to November 7, 2009.

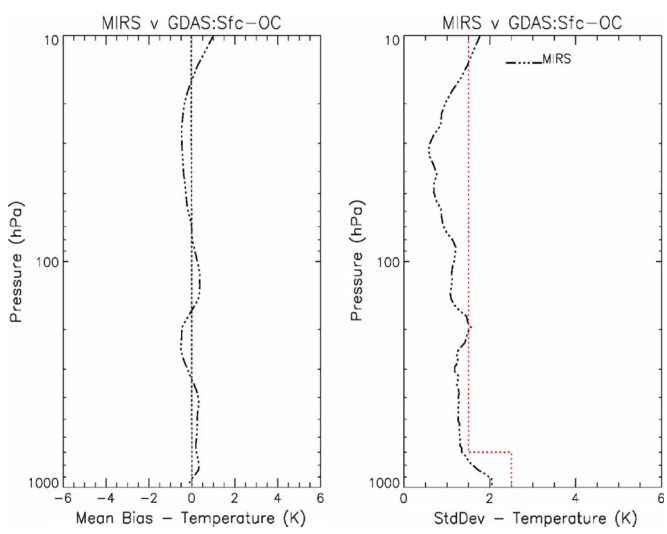

Fig. 12. Temperature profile performances for the ocean case as assessed by comparison to GDAS analyses. The standard deviation is shown at the right panel, while the bias is shown at the left one. The red lines correspond to the predefined requirements set for MiRS.

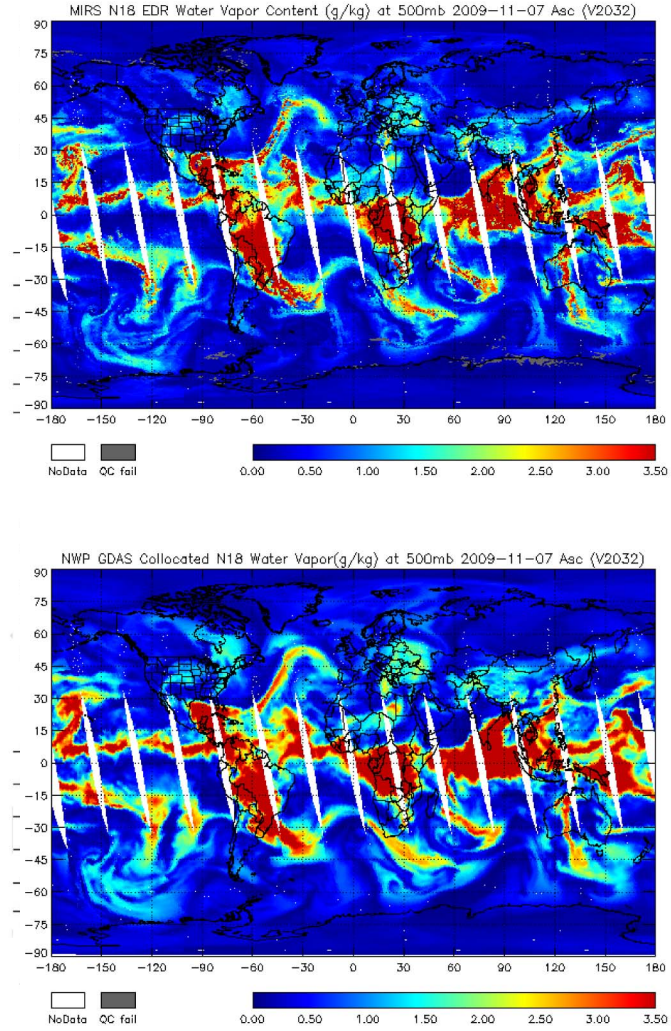

Fig. 13. Global fields of atmospheric moisture at 500-mbar layer (top) as determined by the MiRS algorithm and (bottom) as provided by the GDAS analysis. N18 data from November 7, 2009.

to compute these statistics. Performances of the temperature profile over ocean surfaces from MiRS, when compared to GDAS, are deemed reasonable, with a low bias overall and a low standard deviation, which perhaps has a tendency to increase at the surface and at the tropopause levels as expected but remains within the predefined requirements (see Fig. 12). More assessments of the temperature performances will be summarized in the following validation section by comparing MiRS retrievals to a multitude of reference data sources.

2) Moisture Sounding: The same type of comparison is performed for the vertical atmospheric moisture profiles. Fig. 13 shows maps of the humidity field at the 500-mbar layer as retrieved by MiRS and as provided by the GDAS analysis. From this figure, we can see that the majority of moisture plumes and other large scale features are well captured by MiRS retrievals. A summary of the performances of the water vapor performances, as compared to NWP analyses and radiosondes, will be presented in the following validation section.

3) Emissivity: Another example of the routine monitoring of MiRS retrievals is shown in Fig. 14 for the emissivity product. This figure shows two maps corresponding to the MiRS retrieval at the 50.3-GHz channel (top) and the GDAS-based

This article has been accepted for inclusion in a future issue of this journal. Content is final as presented, with the exception of pagination.

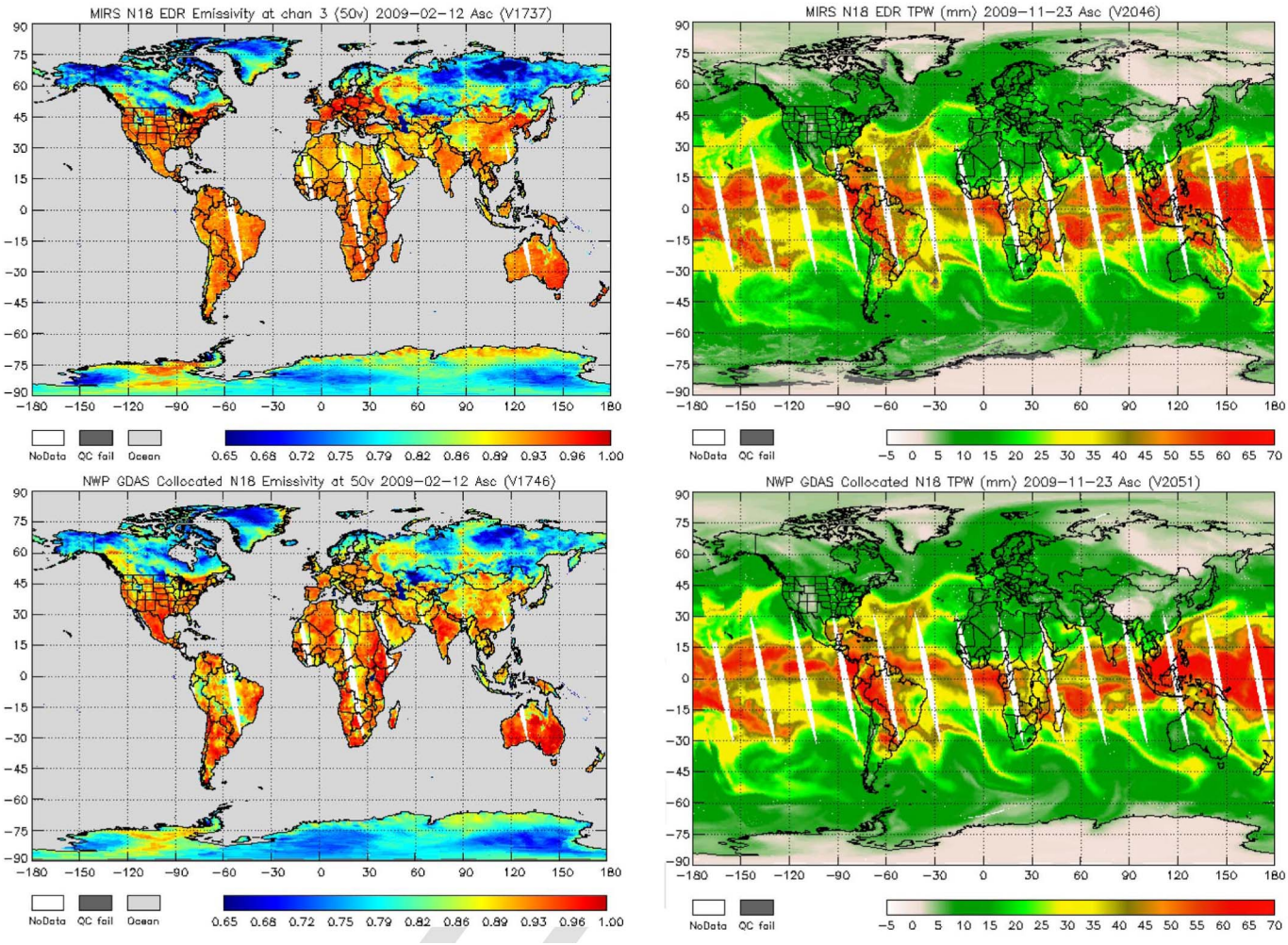

Fig. 14. Global fields of land emissivity for the 50.3-GHz channel (top) as retrieved by the MiRS algorithm and (bottom) as provided by the analytical emissivity based on the GDAS analysis. Field corresponds to February 2, 2009.

analytical emissivity (bottom). A discussion on the methodology that is used to compute the analytical emissivity was provided previously in Section II-D. Globally (only land is shown), MiRS-based emissivity retrievals are very similar to the analytical emissivity, even if the two methods are different and independent.

We could see, however, that the two estimates of emissivities differ in some areas, which could be attributed to the following: 1) the poor accuracy of the skin temperature estimate from GDAS over the high-latitude regions, for instance, where snow and ice cover the surface, and 2) the nonvalidity of the assumptions made to compute the emissivity over mountainous regions or over the Amazon forest where the surface is significantly nonspecular. Note that the accuracy of the analytical emissivity depends strongly on the accuracy of the temperature and moisture information provided, as well as on the skin temperature.

4) TPW Extended Globally: The TPW from MiRS is a simple vertical integration of the water vapor profile, as mentioned earlier. The handling of the surface through the retrieved emissivity vector allowed us to extend the retrieval of the TPW over all surfaces [3], as shown in Fig. 15.

The extended TPW globally (ocean, land, sea ice, snow, and coastal areas) has proved to be a useful product for many applications, including short-term precipitation forecasting and study of the hydrological cycle. Fig. 15 shows that MiRS compares favorably to GDAS in terms of the global distribution

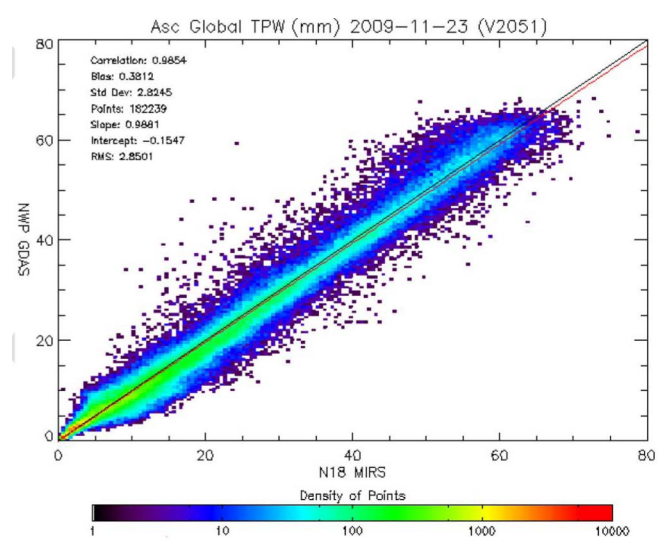

Fig. 15. Performances of the MiRS-based TPW. (Top) MiRS and (middle) GDAS fields compare favorably. (Bottom) Scatterplot between the two presents the statistical performance (globally).

This article has been accepted for inclusion in a future issue of this journal. Content is final as presented, with the exception of pagination.

of the features (frontal systems, moisture plumes, etc.) as well as in terms of statistical performances. The global statistics show an overall bias of 0.38 mm and a standard deviation of 2.82 mm, which are considered reasonable. In a separate study [3], dedicated to the assessment of the TPW global coverage from MiRS, these performances are computed using a number of different reference data sets, and they were stratified by surface background types as well as by sensors. The TPW from MiRS was found to be valid over all surface types, except when there is precipitation. In the presence of precipitation, it is radiometrically difficult to distinguish water vapor signature from liquid water signature.

5) Surface Parameters: A variety of surface properties are retrieved from MiRS. These include the LST, SIC, SWE, and snow cover extent. The latter three cyrospheric parameters are derived explicitly from the MiRS retrieved surface emissivity, as described in Section III-F.2). An example of MiRS LST is shown in Fig. 16. The operational LST refers to skin temperature over snow-free land surfaces only. MiRS also retrieves skin temperature over snow-covered land and nonland (ocean and sea ice) surfaces, but these are not declared operational. The main reason for not declaring those products operational is the fact that limited validation has been performed on them. Another reason is the absence so far of an operational user request. Specifically, Fig. 16 shows the retrieved LST from MiRS NOAA-18 on March 14, 2010, (top) and the comparison to collocated ECMWF analysis (bottom). Overall, the surface temperature from MiRS is consistent with other sources (in this case, skin temperature from ECMWF). Further assessment of LST will be presented in a separate study. Globally, the bias is found to be around 1 K–2 K, and the standard deviation is found to be between 5 K and 6 K. The differences are found to be more pronounced in the high-latitude regions and in areas where snow covers the surface. One must note that skin temperature is expected to be different when measured from the microwave, where the wavelength senses up to a few centimeters inside the soil, and when measured by infrared sensors which tend to be sensitive to the skin temperature only. This penetration depth is dependent on the frequency and on the type of soil, which creates both systematic (biases) and scattered differences that contribute to the overall standard deviation.

Fig. 17 shows an example of SIC retrieved on February 20, 2010, from NOAA-18 data. The figure shows both the MiRS product obtained from ascending passes (top panel) and the product produced from AMSR-E microwave data (middle panel) using the daily product obtained from the NASA Team 2 algorithm [20]. The lower panel shows the corresponding difference field (MiRS-AMSR-E) and indicates that agreement with an independent microwave estimate is quite good, with the largest differences located near the ice edge. This is to be expected since the SIC (or percentage) is typically footprint dependent and since the two sensors being compared here (AMSU and AMSR-E) have definitely different footprint sizes and shapes. This difference is more pronounced at the sea ice edge where heterogeneity is maximal. More details on the MiRS SIC retrievals may be found in [16].

In Fig. 18, SWE is presented, also retrieved on February 20, 2010, from NOAA-18. Again, the MiRS product based on descending passes is shown at the top panel, while the NASA AMSR-E/Aqua Daily Level 3 product [15] is shown at the middle panel. At the bottom panel is the daily operational ice and snow cover IMS analysis produced by the National Ice Center from the Interactive Multisensor Snow and Ice Mapping System [11].

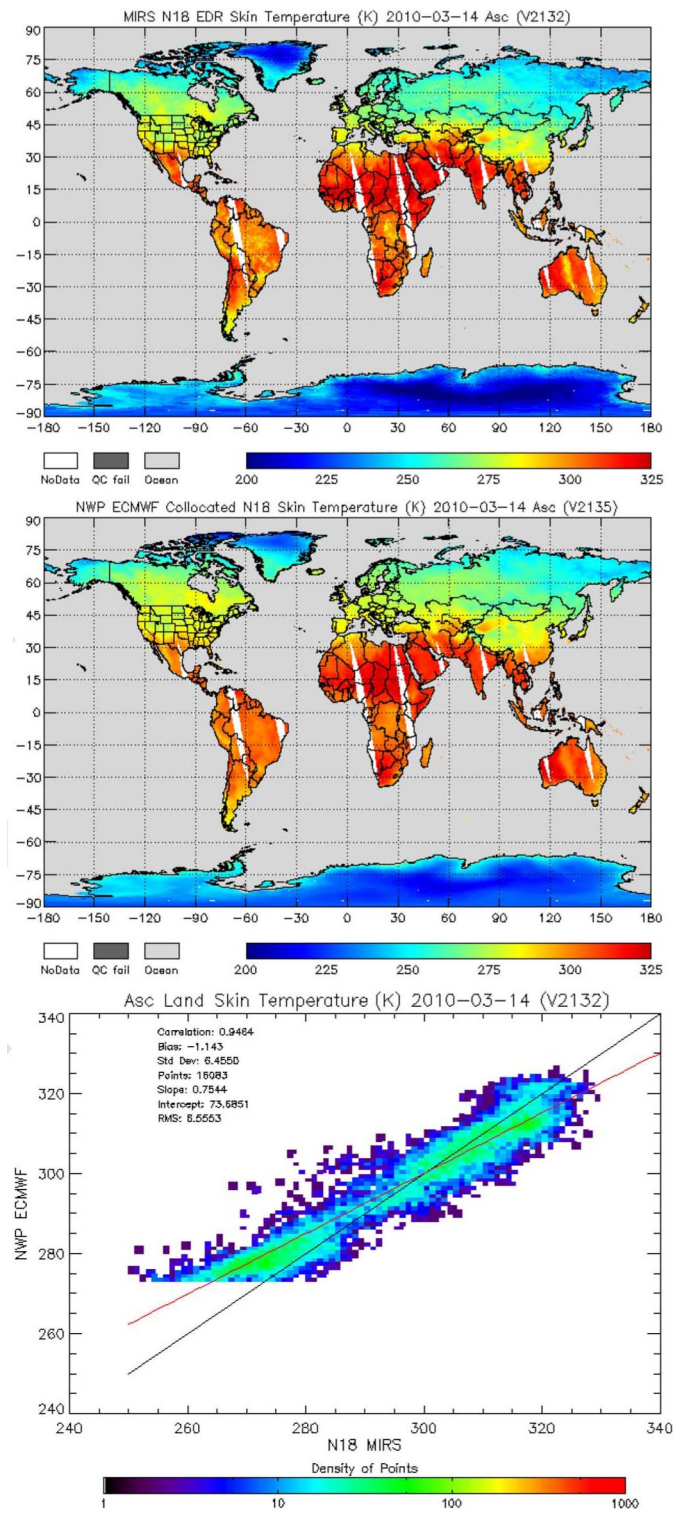

Fig. 16. (Top) LST derived from MiRS using NOAA-18 data on March 14, 2010, for ascending orbits, (middle) field of LST for collocated ECMWF analysis, and (bottom) scatter plot with statistics. Points with subfreezing temperatures were removed from the scatter plot.

This article has been accepted for inclusion in a future issue of this journal. Content is final as presented, with the exception of pagination.

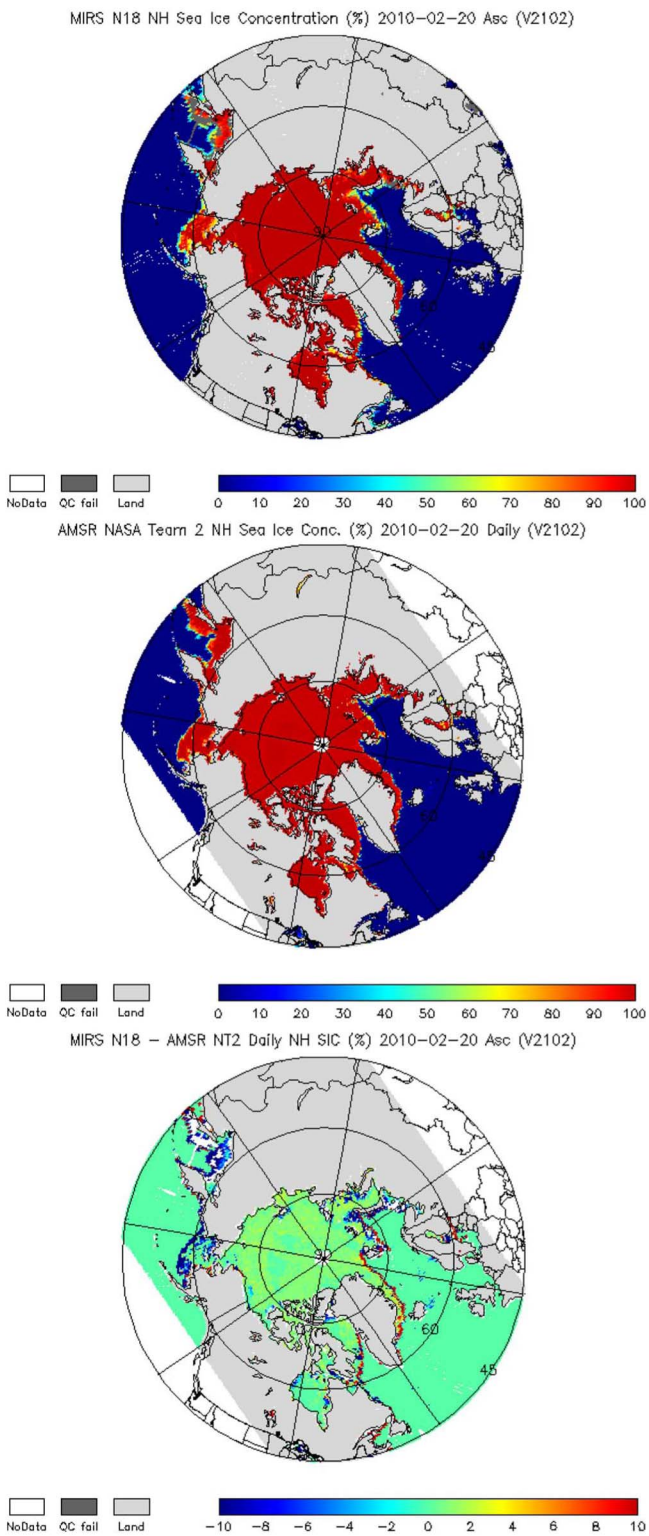

Fig. 17. Example of SIC (percent) retrieved on February 20, 2010. Shown are (top) MiRS algorithm using NOAA-18 data, (middle) AMSR-E NASA Team 2, and (bottom) difference field.

Overall, the products are fairly consistent, with the best agreement over Siberia, presumably due to the less ambiguous signal over the colder, dryer, and deeper snow cover and larger differences over southern areas of the snow pack. A good agreement of the IMS analysis with the SIC retrievals shown in Fig. 17 is also noted.

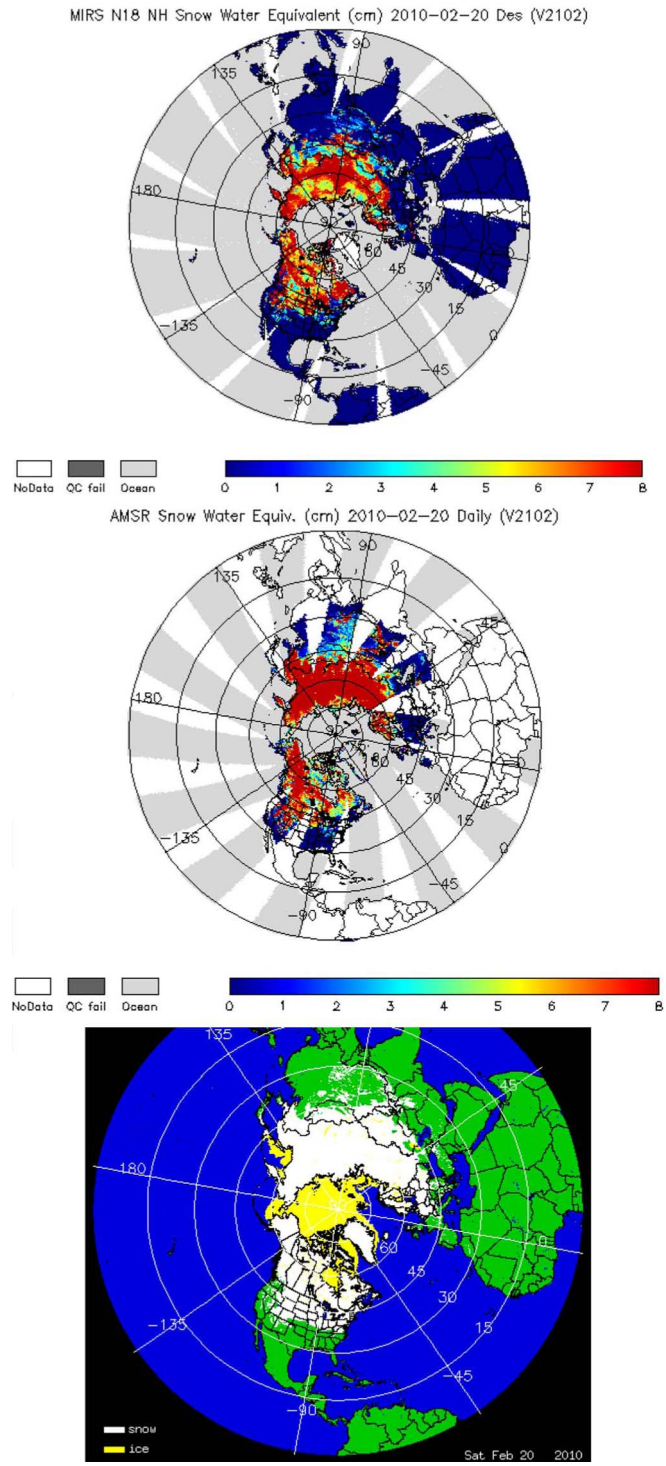

Fig. 18. Example of SWE (in centimeters) retrieved on February 20, 2010, from the (top) MiRS and (middle) NASA Level 3 Daily product. The IMS daily ice and snow cover analysis is shown at the bottom panel.

6) Cloud and Hydrometeor Parameters: As part of the MiRS postprocessing described in Section III-F.3, the MiRS derives the instantaneous RR. Fig. 19 shows a comparison between the daily NOAA/NCEP Climate Prediction Center (CPC) precipitation based on rain gauge analysis and the daily MiRS precipitation estimate (in millimeters per day) generated from the instantaneous RRs derived from NOAA-18, Metop-A,

This article has been accepted for inclusion in a future issue of this journal. Content is final as presented, with the exception of pagination.

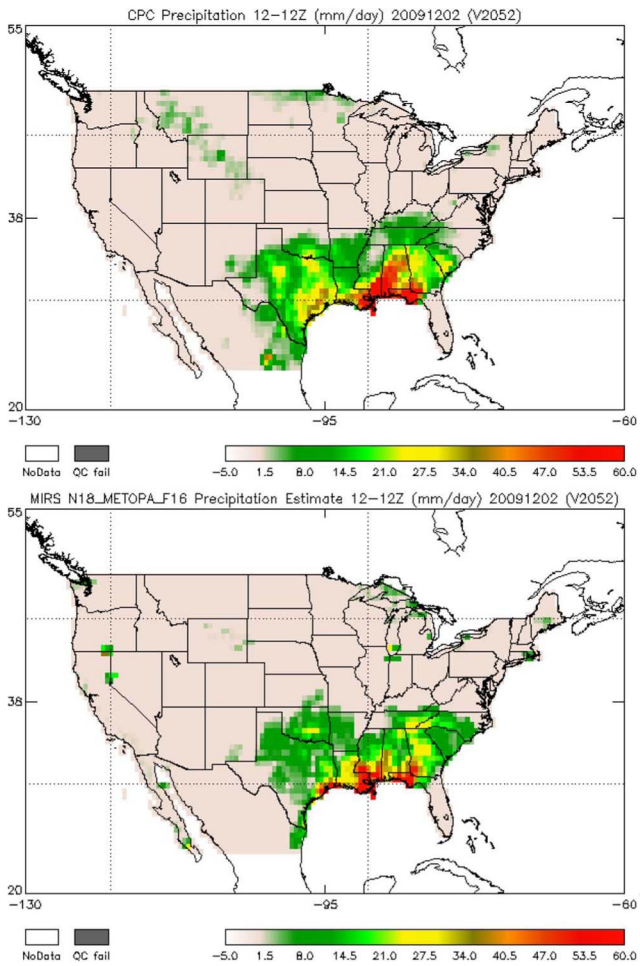

Fig. 19. (Top) Daily CPC precipitation over the CONUS based on rain gauge analysis and (bottom) MiRS precipitation composite based on RR retrievals from NOAA-18, Metop-A, and DMSP-F16.

and DMSP-F16. In this comparison, the limited temporal and spatial coverage associated with the satellite sensors used to generate the MiRS precipitation estimate must be considered, compared to that of the rain gauges. However, it is clear that the MiRS precipitation estimate is able to detect rainfall events with geographical distribution and intensity comparable to those of the CPC analysis.

7) Monitoring of Pentads, Weekly, and Monthly Composites: Another type of monitoring of MiRS products that is performed at NOAA consists of generating pentads, weekly, and monthly composites of global maps from the daily MiRS products.

This time-compositing process allows us to check the slow moving features (seasonal or climatic features) by removing the high-frequency variability, but it also allows us to detect any persistent defects in the MiRS retrievals. Fig. 20 shows the monthly averaged surface emissivity at 89 GHz for February 2008 using NOAA-18, where lower values over northern hemispheric land masses have been influenced by persistent snow cover. Fig. 21 shows the comparison between the MiRS monthly rain composite using NOAA-18 data and the rain composite generated using the Microwave Surface and Precipitation Products System (MSPPS) heritage algorithm [9] which MiRS is scheduled to gradually replace in the next couple of

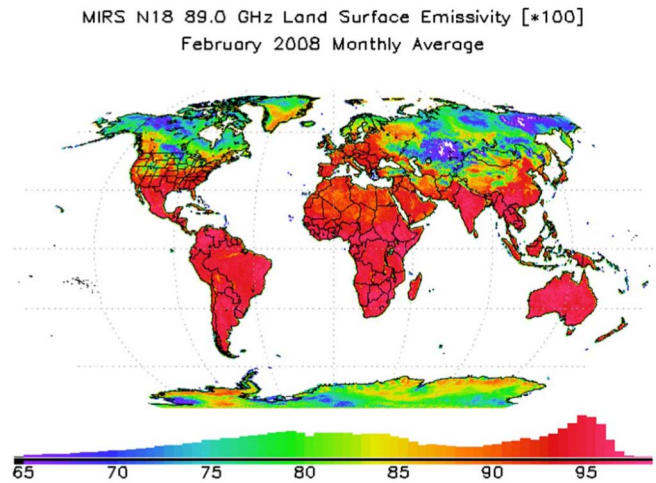

Fig. 20. Monthly average of MiRS land emissivity at the 89-GHz channel. Data correspond to February 2008 obtained from NOAA-18 AMSU/MHS sensors.

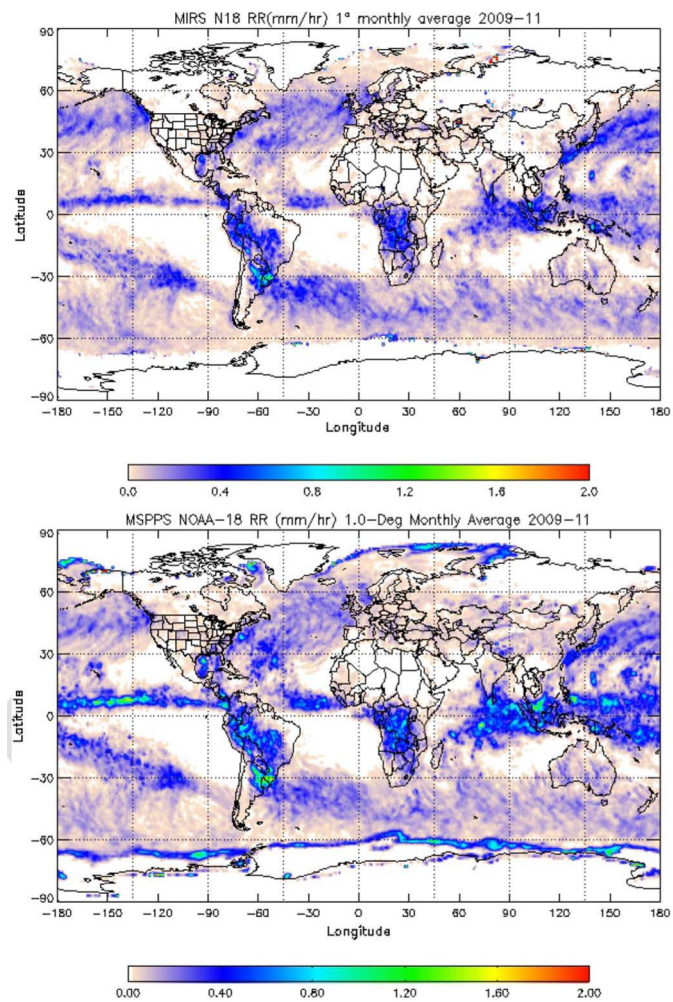

Fig. 21. Comparison of two monthly composites of RR from the (top) MiRS and (bottom) heritage algorithm MSPPS. Notice the significantly reduced false alarms at the sea ice edges by the MiRS algorithm. The unit is in millimeters per hour. Both composites are based on NOAA-18 data.

years. The compositing is done at different spatial resolutions (1° or 2.5°) and is performed on all sensors for which MiRS is applicable. The original resolution of the MiRS retrieval is

This article has been accepted for inclusion in a future issue of this journal. Content is final as presented, with the exception of pagination.

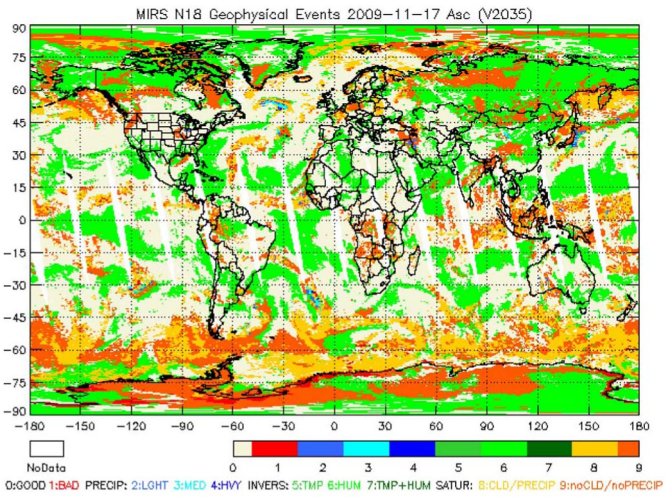

Fig. 22. Global map depicting different information and flags as they relate to the outputs of MiRS. Note that some flags are not exclusive, and therefore, the color visible is not indicative of only one flag being turned on.

that of AMSU, as mentioned earlier, but the MSPPS original resolution is that of MHS. We could see in this figure that the persistent false alarm at the sea ice edges is pretty clear in the MSPPS algorithm. This is due to the mixed signal in the brightness temperatures for which the algorithm is not trained. The MiRS algorithm dramatically reduces this issue, as shown in Fig. 21, due to the fact that the emissivity is part of the state vector, making the emissivity as the proxy product that takes in the mixed signal (instead of the atmospheric parameters).

8) Quality Control: In addition to the convergence metric mentioned earlier, which is an excellent tool to determine if anything is inconsistent between the measurements and the solution found, a number of other flags and indicators are also part of the MiRS outputs. Fig. 22 shows a global map of those flags and corresponding values. They indicate profiles where the retrieval was nominal or had no meteorological event as zero; where a bad retrieval or poor quality measurements as one; where precipitation was detected (light, medium, or heavy as two, three, and four, respectively); where a vertical inversion was found in temperature and/or humidity as five, six, and seven; and where supersaturation occurred in clear sky as eight and cloud or precipitating sky as 9. In addition, several quality assessment parameters are optionally computed within MiRS, but they are not displayed here. These are the uncertainty matrix S, the contribution function D, and the average Kernel A. The formulation of these quality-control metrics is given in the following:

$$S = B - B \times K^T (K \times B \times K^T + E)^{-1} \times K \times B$$

$$D = B \times K^T (K \times B \times K^T + E)^{-1} \times (Y(X) - K \times X_0)$$

$$A = D \times K.$$

These parameters could be useful for NWP applications and blending techniques since they provide objective information about the uncertainties of the retrievals and the radiometric information content used on a point-to-point basis.

TABLE IV
SUMMARY OF THE MiRS-BASED TEMPERATURE PROFILE PERFORMANCES (BIAS AND STANDARD DEVIATION IN KELVIN) WHEN COMPARED TO ECMWF AND GDAS ANALYSES AS WELL AS TO OPERATIONAL RADIOSONDES. SEE TEXT FOR MORE DETAILS

		Ocean		Land	
	Layer	Bias (K)	Std (K)	Bias (K)	Std (K)
MIRS vs ECMWF	100 mb	0.2	1.8	1.0	1.8
	300 mb	0.2	1.5	0.5	1.7
	500 mb	0.1	1.3	0.2	1.8
	800 mb	1.2	1.8	1.2	3.4
	950 mb	1.7	2.7	0.9	4.5
MIRS vs GDAS	100 mb	0.0	1.5	0.0	1.7
	300 mb	0.2	1.6	0.2	1.8
	500 mb	-0.2	1.4	0.2	1.8
	800 mb	1.2	1.7	1.3	3.8
	950 mb	1.1	2.8	0.9	4.8
MIRS vs RAOB	100 mb	0.1	1.7	0.3	2.1
	300 mb	0.9	1.9	0.5	1.8
	500 mb	0.1	1.6	-0.1	1.8
	800 mb	0.7	2.1	1.5	2.8
	950 mb	0.8	2.9	1.7	3.1

B. Validation

This section will present a number of validation results for some of the MiRS parameters. It will not go into extensive details which may be found in current or future publications [4], [13], [16]. It complements the previous section related to routine monitoring of MiRS performances. Some of the routine performances (computed against NWP analyses for instance) will also be summarized in table format in this section.

1) Temperature and Moisture Sounding: The performances of the MiRS-based temperature and moisture sounding profiles are presented in Tables IV and V, respectively. They are stratified by ocean and land surface types and are given at five different atmospheric layers corresponding to 100, 300, 500, 800, and 950 mbar for temperature comparison and four layers for moisture sounding since the 100-mbar layers are not reliable from the reference data, particularly radiosonde. Note, however, that all layers have been assessed. This is the only snapshot of those performances. We notice that temperature biases are relatively consistent whether we use ECMWF or GDAS as a reference. The biases over the ocean are below 1 K and above 500 mbar and tend to increase slightly at the surface to 1.7 K and 1.1 K for ECMWF and GDAS, respectively. Over land, they are roughly the same (within a half degree margin).

The uncertainty of the temperature profile, measured by the statistical standard deviation of the differences between the reference data and MiRS retrievals, is also consistent between ECMWF and GDAS. Over the ocean, it varies between 1.8 K at 100 mbar and 2.7 K at 950 mbar and between 1.5 K at 100 mbar and 2.8 K at 950 mbar for ECMWF and GDAS, respectively. Over land, it varies between 1.8 K at 100 mbar and 4.5 K at 950 mbar and between 1.7 K at 100 mbar and

This article has been accepted for inclusion in a future issue of this journal. Content is final as presented, with the exception of pagination.

TABLE V
SUMMARY OF THE MiRS-BASED MOISTURE PROFILE PERFORMANCES (RELATIVE BIAS AND RELATIVE STANDARD DEVIATION IN PERCENTAGE OF THE REFERENCE WATER VAPOR AMOUNTS) WHEN COMPARED TO ECMWF AND GDAS ANALYSES AS WELL AS TO OPERATIONAL RADIOSONDES. SEE TEXT FOR MORE DETAILS

		Ocean		Land	
	Layer	Bias (%)	Std (%)	Bias (%)	Std (%)
MIRS vs ECMWF	300 mb	8.0	41.0	1.5	54.0
	500 mb	-0.5	42.5	-1.5	41.0
	800 mb	11.0	28.0	-1.0	32.5
	950 mb	-5.0	17.0	-5.5	32.0
MIRS vs GDAS	300 mb	-29	40.5	-30.0	53.0
	500 mb	-10.0	39.5	-15.0	38.5
	800 mb	2.0	22.0	8.0	30.0
	950 mb	-5.5	13.5	3.0	30.0
MIRS vs RAOB	300 mb	21.5	75.0	21.0	83.0
	500 mb	2.0	65.0	1.0	60.0
	800 mb	2.0	38.0	7.0	41.0
	950 mb	0.5	21.5	4.0	30.0

4.8 K at 950 mbar for ECMWF and GDAS, respectively. This indicates a higher uncertainty in temperature near the surface. Note that only temperature profiles over the ocean are officially declared operational. When we analyze the comparison to the radiosondes data, the results are not similar. The biases are slightly lower at the surface for the ocean and slightly higher at the surface for the land comparison. The standard deviation over the ocean is consistent with that obtained using ECMWF and GDAS, but the uncertainty over land is slightly lower than what was obtained with ECMWF and GDAS (3.1 K instead of 4.5 K and 4.8 K at the surface).

The disparity of the results is more striking for the case of the water vapor performances, as could be seen in Table V.

The standard deviation over both land and ocean is consistent between the comparisons made with ECMWF and those made with GDAS, ranging between 41% at 300 mbar and around 13.5% at the surface for the ocean case and ranging between 54% at 300 mbar and 30% at the surface for the case of land. The bias, however, is not consistent between the ECMWF and GDAS assessments for both ocean and land cases. It is also different from the assessment results obtained when comparing to radiosondes. The uncertainty computed using the radiosondes as a reference is similar at the surface with that obtained using ECMWF or GDAS, but it diverges to higher uncertainty values at higher altitudes.

The inconsistency in the results, especially between using NWP analyses (ECMWF or GDAS) and radiosondes, suggests that there is intravariability between the different references used. This makes us conclude that MiRS performances are well within the uncertainty of all of the reference data taken together. If there is a systematic difference found in MiRS, it would, in theory, appear in all comparisons.

2) Surface Properties (Emissivity, SWE, and SIC): The surface properties were also assessed thoroughly using several reference data from the analytical emissivities and the MSPPS algorithm for the emissivity product to the AMSR-E data and other ground-based measurements for SIC and SWE. Table VI summarizes, for instance, the stratified performances over land and snow and over sea and ice (bias and standard deviation) of the MiRS emissivity when compared to the analytically derived emissivity for NOAA-18 AMSU channels (50.3 and 23.8 GHz, respectively). These results indicate that emissivity biases are relatively small (around or less than 1%) and that standard deviations vary between 2% and 3% depending on the channel and the surface type. Higher frequency channels, which are more sensitive to atmospheric contamination (specifically cloud), have higher uncertainties (not shown here) but are still retrieved with a reasonable accuracy since they are spectrally constrained with the emissivity covariance matrix and by the simultaneous retrieval of the atmospheric products.

TABLE VI
ASSESSMENT OF THE 23.8- AND 50.3-GHz EMISSIVITY PERFORMANCES FOR SEA AND ICE FOR THE FORMER (RIGHT) AND FOR LAND AND SNOW FOR THE LATTER (LEFT)

50.3 GHz	Std Dev	Bias
Land	0.03	0.000
Snow	0.03	0.012

23.8 GHz	Std Dev	Bias
Sea	0.03	0.003
Ice	0.02	0.001

The SWE retrieved by MiRS, which is based on the post-processing described in Section III-F and is applied to the retrieved emissivities, was compared to a number of reference data sources including the AMSR-E, the Interactive Multi-sensor Snow and Ice Mapping System (IMS), and the Naval Research Laboratory's algorithm (for SSMI/S case). It was also compared to ground-based snow property measurements made in Northern Canada in 2003. Fig. 23 shows the results of this comparison along with the comparison between the heritage algorithm MSPPS with the same reference data set. The biases are relatively similar, but the rms error was decreased by MiRS from 4 to 3.4 cm, and the correlation was increased from 35% to 52%. It is important to note that the verification of the emissivity-based products from MiRS (such as the SWE or the SIC) also constitutes an indirect validation of the emissivity product itself.

The MiRS SIC retrieval is based on the inverted emissivity spectrum. The postprocessing uses the absolute amplitude of the spectrum and/or the relative spectral slopes between the channels (i.e., the shape of the spectrum). Using the spectral shape was found to be more robust in some instances than using solely the magnitude of the emissivity spectrum. We should note that the postprocessing step that interprets the emissivity spectrum into SIC (and snow properties) also uses the surface temperature from MiRS to help exclude the presence of frozen water, therefore reducing the rate of false alarms.

The SIC product from MiRS was compared to a multitude of reference data, including the official NASA-T2 and NASA-Bootstrap algorithms, showing that MiRS generally captures the same extent of sea ice coverage. This was shown in the previous section. Another consistency check was performed to qualitatively assess the validity of the SIC from MiRS. In this test, a region in the Antarctic was selected because it is known as being fully covered with sea ice all year long (latitude

This article has been accepted for inclusion in a future issue of this journal. Content is final as presented, with the exception of pagination.

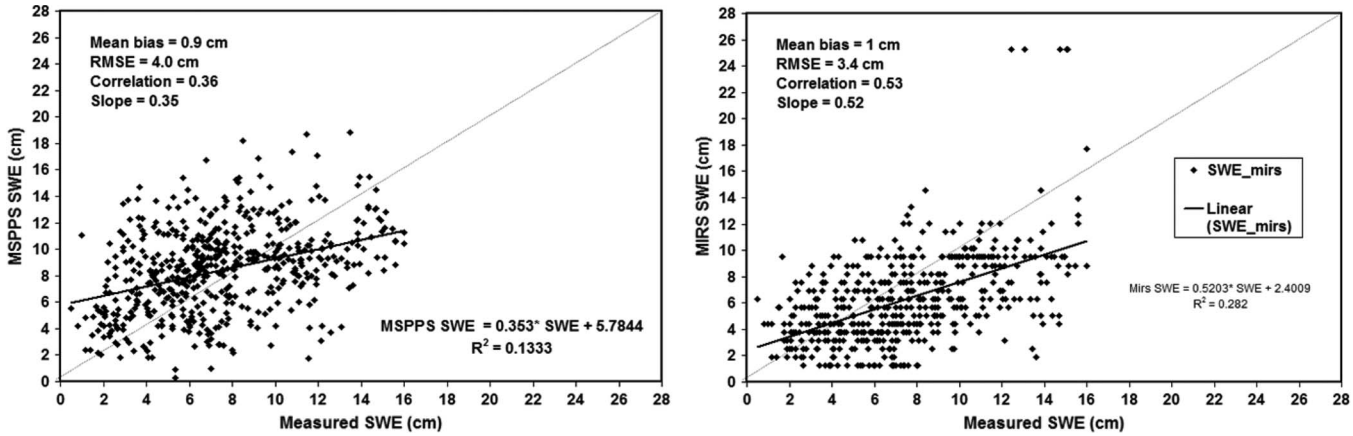

Fig. 23. Comparisons between the ground-based snow measurements and the retrievals of the new MiRS emissivity-based SWE algorithm (bottom panel). The same comparison, but using the heritage algorithm MSPPS (brightness temperature based), is also shown (top). The results show improved statistics with the new technique.

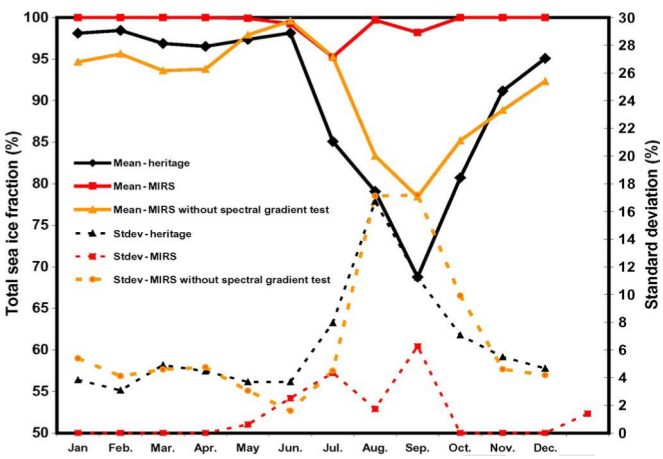

Fig. 24. Time series of SIC in 2006 from MiRS and MSPPS. Data correspond to a region in the Antarctic known as being fully covered with sea ice all-year long. Black lines correspond to MSPPS SIC, and red and orange lines correspond to MiRS (using the spectral slope (more robust) or not, respectively). Solid lines refer to absolute SIC, while dashed lines refer to the standard deviations.

84–86 N and longitude 135–137 W). Data taken in 2006 (January to December) were gathered to assess the time series. SIC from MiRS, using the magnitude of the spectrum and the more robust approach based on the spectral shape, and data from the heritage algorithm MSPPS were plotted (see Fig. 24). Ideally, the SIC all-year long should be close to full coverage (100%). Both the SIC absolute value (in solid lines) and the standard deviation (in dashed lines) are plotted. MiRS retrieved a SIC that is remarkably close to 100%, with a low standard deviation. All algorithms tend to have some uncertainty during the melting season (summer) where the signal could be misinterpreted. The fact that the emissivity spectral shape is used makes it less likely to miss the ice signal, given that the ice spectrum (when all channels are used), even if mixed with a melted top layer, is easily distinguishable from the ocean spectrum. Algorithms based on the absolute magnitude of the brightness temperatures (or the emissivities) or algorithms that use just one or two channels (with less knowledge about the full spectral shape) are more likely to have difficulties in these conditions.

3) Clouds and Hydrometeor Parameters: These parameters include the CLW, IWP, RWP, and surface RR. These hydrometeor parameters are notoriously difficult to assess because of the multitude of unknowns mentioned already in Section III-F. They are also difficult to assess because of the inexistence of an effective way to measure these quantities (from either ground-based or airborne sensors). The easiest to assess among these hydrometeor parameters is the surface RR, which could be compared to both ground-based meteorological radars as well as to other algorithms (and other sensors) and surface-based rain gauges. We will therefore concentrate this section on the RR assessment. It is important to note that the postprocessing stage (in MiRS) that leads to RR uses IWP, CLW, and IWP, among others, as inputs, and therefore, assessing RR is an indirect assessment of these inputs, which are, as expressed already, hard to assess individually given the lack of reference data. The rain rate from MiRS was assessed internally using Tropical Rainfall Measuring Mission (TRMM) and CLOUDSAT retrievals, ground-based gauges, and radars. It was also assessed independently through the International Precipitation Working Group (IPWG) program, where MiRS retrievals are compared against reference data (radars and gauges) along with other algorithms (infrared and microwave or combination thereof) using the exact same methodology. In this paper, we will present short summaries of those two assessments.

Fig. 25 shows one aspect of the assessment of MiRS rainfall performed at NOAA, using the CPC rain gauges analyses as a reference. MiRS-based retrievals of RR from different sensors (NOAA-18, Metop-A, and DMSP-F16 SSMI/S) are assessed individually, as well as the composite precipitation that uses RR samples from three sensors combined. This comparison with CPC is limited to the CONUS. The bias is centered around zero with a margin of ± 2 mm/h. The correlation is higher when all sensors are combined together and is centered around 60%. This correlation and other metrics were found to be comparable to those of other more established algorithms, such as the TRMM-based GPROF algorithm which is also assessed within the IPWG [8]. This higher correlation of the sensor composite (as opposed to the individual sensors) is due to the higher temporal and spatial coverage obtained with combining

This article has been accepted for inclusion in a future issue of this journal. Content is final as presented, with the exception of pagination.

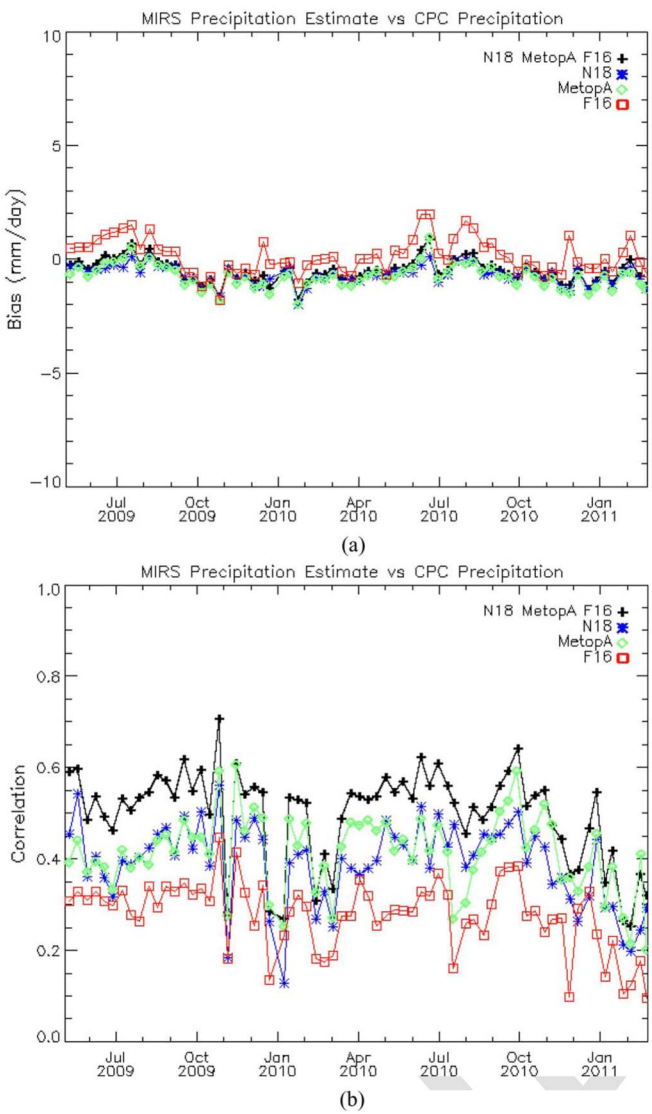

Fig. 25. Time series of the MiRS RR performances [(a) bias and (b) spatial correlation] assessed against the CPC rain analyses. MiRS RRs from different individual sensors, as well as from the composite of all sensors, are shown.

all sensors. For the same reason, we notice that the correlation of the individual sensor DMSP-F16 SSMI/S is lower than that of the other sensors (NOAA-18 and Metop-A). Indeed, DMSP-F16 SSMI/S has a narrower swath than those of NOAA-18 and Metop-A, which makes its spatial coverage less optimal, leading to a lower degree of correlation. Intuitively, we do expect that, if the temporal and spatial coverage of a sensor is lower, then the likelihood of missing rain events is higher, which would lead to degraded performances when comparing daily rain estimates. This does not mean that MiRS applied to DMSP-F16 SSMI/S leads to lower quality RRs per se (the retrieval algorithm is the same applied to all sensors). In fact, when computing the same metrics (correlations, biases, etc.) on a set of temporally and spatially collocated profiles (between rain gauges and MiRS retrievals), in which the spatiotemporal coverage is no longer relevant, the same types of performances were found for all sensors.

Fig. 26 shows a summary of the independent assessments of the MiRS RR made within the IPWG. Note that three IPWG sites are currently including MiRS into their intercomparison efforts: the North American, the South American, and the Australian sites.

The assessment is done using rain gauge analyses from CPC and ground-based radars when available. A number of statistical performances are computed, including the spatial correlation, the absolute bias, the rms error, the probability of detection, the false alarm rate, etc. In Fig. 26, we could see that MiRS generally captures the rain events pretty well and that the statistics obtained are comparable to those more established algorithms with similar temporal and spatial coverage.

V. CONCLUSION

A 1DVAR retrieval algorithm has been developed to retrieve a comprehensive suite of geophysical parameters from spaceborne microwave measurements. The suite of parameters consists of those parameters that most directly impact the measurements: atmospheric profiles of temperature, moisture, liquid and ice cloud, liquid precipitation, and surface emissivity spectrum and its skin temperature. In addition, the suite of parameters includes a set of derived products. Some of which are a simple vertical integration of the fundamental profiles, and some others are based on a more elaborate postprocessing. These include surface parameters such as snow cover, SWE, snow effective grain size, SIC, sea ice type/age, and atmospheric parameters such as TPW, CLW, RWP, IWP, and RR. The design of the MiRS algorithm is generic, and it could accommodate any microwave sensor that could be handled by the forward operator CRTM. It is currently operational for NOAA-18, NOAA-19, Metop-A, and DMSP-F16 SSMI/S and is being prepared to run operationally for NPP/ATMS. At the time of writing this paper, MiRS is also being extended to F18 SSMI/S which was launched in late 2009. It also runs experimentally for AMSR-E (imager only) on a daily basis. A large effort has been put into the assessment of all of the products generated by MiRS. This paper has presented a general overview of the algorithm approach and a snapshot of the assessment results. Its goal was to make potential users aware of the availability of these operational products. It is thought that having the same algorithm applied to all microwave sensors will bring consistency between retrievals with an obvious advantage for climate applications. It also reduces significantly the amount of time needed to develop an algorithm for a new sensor. It is noteworthy that, in MiRS, the same code is used for all sensors, as well as the same atmospheric covariance, background, and forward model. Therefore, applying MiRS to a new sensor comes with a high degree of confidence stemming from the previous tuning, improvement, and assessment performed for the previous sensors. Other individual studies have been (or will be) published that address in more detail the validity of individual parameters.

Besides the availability of MiRS products on a real-time basis, the software package itself is also available, and it could be requested, subject to a free-of-charge licensing agreement.

One suggested application of the MiRS package is as a preprocessor for NWP variational data assimilation (3DVAR or

This article has been accepted for inclusion in a future issue of this journal. Content is final as presented, with the exception of pagination.

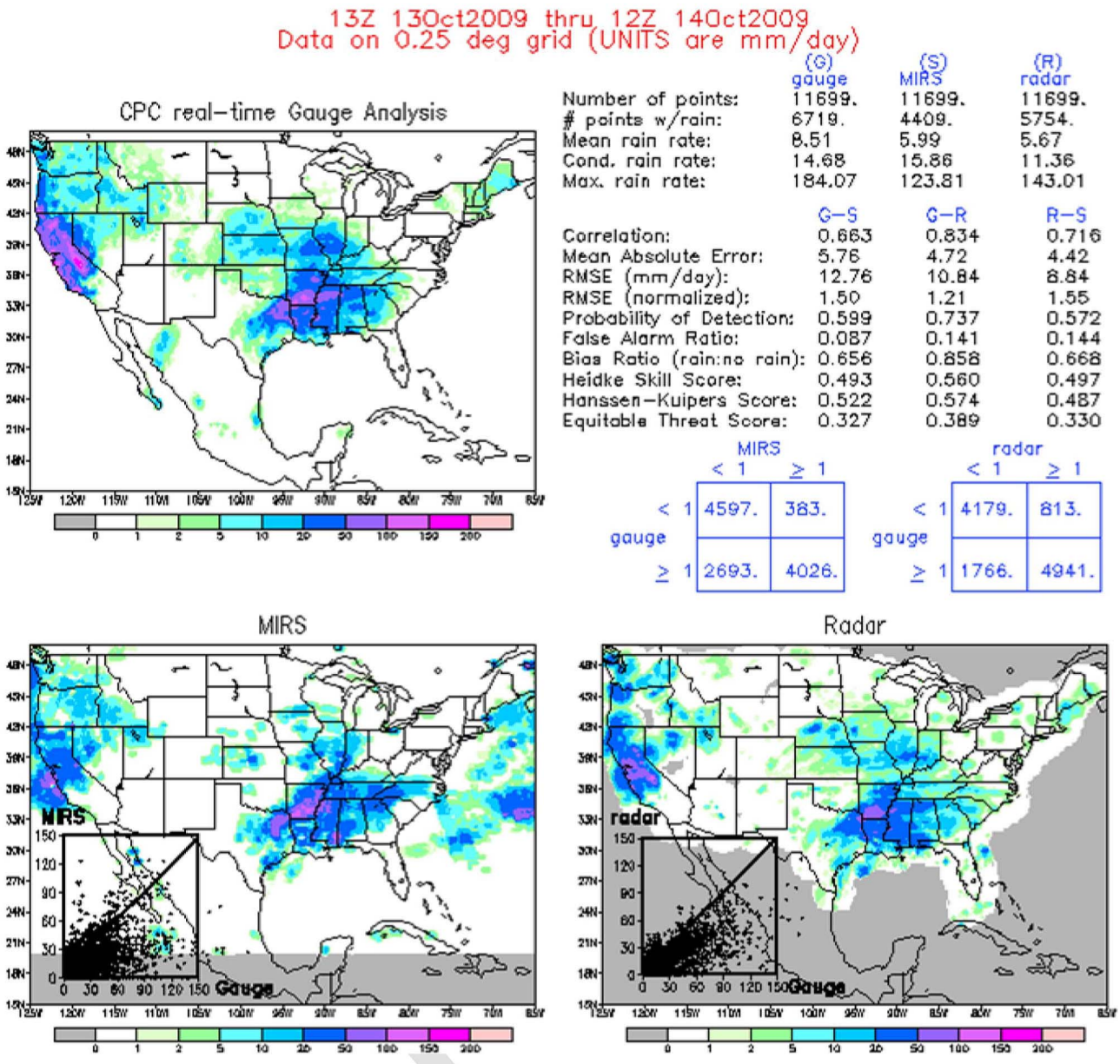

Fig. 26. Snapshot of the independent assessment of MiRS RR performed in the framework of the IPWG. Photograph is courtesy of J. Janowiak from the University of Maryland.

4DVAR). This could serve as a quality-control filter and/or as a tool to provide first estimates of the solution. An additional, perhaps more interesting, application is the adoption of the methodology used in MiRS in handling the surface-sensitive channels and in assimilating cloud/hydrometeors-impacted radiances.

All figures of this paper were taken from the official MiRS Web site which may be accessed for more details about the project, the assessment, and the monitoring of MiRS products (http://mirs.nesdis.noaa.gov).

Acknowledgment

The authors would like to thank the JCSDA CRTM team for providing an early version of the radiative transfer model CRTM, T. Zhu from NOAA/NESDIS for providing MM5 runs for building a covariance matrix for hydrometeors, J. Janowiak and D. Vila from the University of Maryland, and B. Ebert from the Australian Bureau of Meteorology Research Centre for processing MiRS RRs within the IPWG and for providing an independent validation of MiRS precipitation. The views expressed here are those of the authors solely and do not constitute a statement of policy, decision, or position on behalf of NOAA or the U.S. Government.

References

[1] W. Bell, S. English, B. Candy, N. Atkinson, F. Hilton, S. Swadley, W. Campbell, N. Bormann, G. Kelly, K. Masahiro, and N. Baker, "The assimilation of SSMIS radiances in numerical weather prediction models," *IEEE Trans. Geosci. Remote Sens.*, vol. 46, no. 4, pp. 884–900, Apr. 2008.

[2] S.-A. Boukabara, F. Weng, and Q. Liu, "Passive microwave remote sensing of extreme weather events using NOAA-18, AMSUA and MHS," *IEEE Trans. Geosci. Remote Sens.*, vol. 45, no. 7, pp. 2228–2246, Jul. 2007.

This article has been accepted for inclusion in a future issue of this journal. Content is final as presented, with the exception of pagination.

[3] S.-A. Boukabara and F. Weng, "Microwave emissivity over ocean in all-weather conditions, validation using WindSAT and airborne GPS-dropsondes," *IEEE Trans. Geosci. Remote Sens.*, vol. 46, no. 2, pp. 376–384, Feb. 2008.

[4] S.-A. Boukabara, K. Garrett, W. Chen, Q. Liu, B. Yan, and F. Weng, "Global coverage of total precipitable water using a microwave variational algorithm," *IEEE Trans. Geosci. Remote Sens.*, vol. 48, no. 10, pp. 3608–3621, Oct. 2010.

[5] F. Chevallier, "Sampled databases of 60-level atmospheric profiles from the ECMWF analyses," Eur. Centre Medium-Range Weather Forecasts, Reading, U.K., Document No. NWPSAF-EC-TR-004, v. 1.0, 2002.

[6] B. A. Colle, J. B. Olson, and J. S. Tongue, "Multiseason verification of the MM 5. Part II: Evaluation of high-resolution precipitation forecasts over the Northeastern United States," *Wea. Forecast.*, vol. 18, no. 3, pp. 458–480, 2003.

[7] G. Deblonde and S. English, "One-dimensional variational retrievals from SSMI/S-simulated observations," *J. Appl. Meteorol.*, vol. 42, no. 10, pp. 1406–1420, Oct. 2003.

[8] E. E. Ebert, J. E. Janowiak, and C. Kidd, "Comparison of near-real-time precipitation estimates from satellite observations and numerical models," *Bull. Amer. Meteorol. Soc.*, vol. 88, no. 1, pp. 47–64, Jan. 2007.

[9] R. R. Ferraro, F. Weng, N. C. Grody, L. Zhao, H. Meng, C. Kongoli, P. Pellegrino, S. Qiu, and C. Dean, "NOAA operational hydrological products derived from the Advanced Microwave Sounding Unit," *IEEE Trans. Geosci. Remote Sens.*, vol. 43, no. 5, pp. 1036–1049, May 2005.

[10] G. A. Grell, J. J. Dudhia, and D. R. Stauffer, "A description of the fifth-generation Penn State/NCAR Mesoscale Model (MM5)," Nat. Center Atmos. Res., Boulder, CO, NCAR Tech. Note NCAR/TN-398, Jun. 1995.

[11] S. R. Helfrich, D. McNamara, B. H. Ramsay, T. Baldwin, and T. Kasheta, "Enhancements to, and forthcoming developments in the Interactive Multisensor Snow and Ice Mapping System (IMS)," *Hydrol. Process.*, vol. 21, no. 12, pp. 1576–1586, Jun. 2007.

[12] *Integrated Forecast System Documentation Part II: Data Assimilation*, Eur. Centre Medium Range Weather Forecasts, Reading, 2007.

[13] F. Iturbide-Sanchez, S.-A. Boukabara, R. Chen, K. Garrett, C. Grassotti, W. Chen, and F. Weng, "Assessment of a variational inversion system for rainfall rate over land and water surfaces," *IEEE Trans. Geosci. Remote Sens.*, Jan. 2011. DOI: 10.1109/TGRS.2011.2119375, to be published.

[14] F. Karbou, C. Prigent, L. Eymard, and J. Pardo, "Microwave land emissivity calculations using AMSU measurements," *IEEE Trans. Geosci. Remote Sens.*, vol. 43, no. 5, pp. 948–959, May 2005.

[15] R. E. J. Kelly, A. T. C. Chang, J. L. Foster, and M. Tedesco, *AMSR-E/Aqua Daily L3 Global Snow Water Equivalent EASE-Grids*. Boulder, CO: Nat. Snow Ice Data Center, Digital Media, 2004, updated daily.

[16] C. Kongoli, S.-A. Boukabara, B. Yan, F. Weng, and R. Ferraro, "A new sea-ice concentration algorithm based on microwave surface emissivities," *IEEE Trans. Geosci. Remote Sens.*, vol. 49, no. 1, pp. 175–189, Jan. 2011.

[17] D. B. Kunkee, G. A. Poe, D. J. Boucher, S. Swadley, Y. Hong, J. Wessel, and E. Uliana, "Design and evaluation of the first Special Sensor Microwave Imager/Sounder (SSMIS)," *IEEE Trans. Geosci. Remote Sens.*, vol. 46, no. 4, pp. 863–883, Apr. 2008.

[18] Q. Liu and F. Weng, "Advanced doubling-adding method for radiative transfer in planetary atmospheres," *J. Atmos. Sci.*, vol. 63, no. 12, pp. 3459–3465, Dec. 2006.

[19] A. C. Lorenc, "Development of an operational variational assimilation scheme," *J. Meteorol. Soc. Jpn.—Special Issue "Data Assimilation in Meteorology and Oceanography: Theory and Practice"*, vol. 75, no. 1B, pp. 339–346, 1995.

[20] T. Markus and D. J. Cavalieri, "An enhancement of the NASA Team sea ice algorithm," *IEEE Trans. Geosci. Remote Sens.*, vol. 38, no. 3, pp. 1387–1398, May 2000.

[21] L. M. McMillin, L. J. Crone, and T. J. Kleespies, "Atmospheric transmittance of an absorbing gas. 5. Improvements to the OPTRAN approach," *Appl. Opt.*, vol. 34, no. 36, pp. 8396–8399, Dec. 1995.

[22] T. Mo, "Calibration of the Advanced Microwave Sounding Unit-A radiometers for NOAA-N and NOAA-N′," U.S. Dept. Commerce, Nat. Ocean. Atmos. Admin., Nat. Environ. Satellite, Data, Inf. Service, Silver Spring, MD, Tech. Rep. NOAA NESDIS 106, 2002.

[23] J.-L. Moncet, S. A. Boukabara, A. Lipton, J. Galantowicz, H. Rieu-Isaacs, J. Hegarty, X. Liu, R. Lynch, and N. Snell, *Algorithm Theoretical Basis Document (ATBD) for the Conical-Scanning Microwave Imager/Sounder (CMIS) Environmental Data Records*, vol. 2, *Core Physical Inversion Module*. Lexington, MA: AER Inc., Mar. 2001, ver. 1.4.

[24] C. Prigent, W. B. Rossow, and E. Matthews, "Microwave land surface emissivities estimated from SSM/I observations," *J. Geophys. Res.*, vol. 102, no. D18, pp. 21 867–21 890, 1997.

[25] W. L. Smith and H. M. Woolf, "The use of eigenvectors of statistical covariance matrices for interpreting satellite sounding radiometer observations," *J. Atmos. Sci.*, vol. 33, no. 7, pp. 1127–1140, Jul. 1976.

[26] F. Weng, B. Yan, and N. C. Grody, "A microwave land emissivity model," *J. Geophys. Res.*, vol. 106, no. D17, pp. 20 115–20 123, 2001.

[27] F. Weng, Y. Han, P. Van Delst, Q. Liu, T. Kleespies, B. Yan, and J. Le Marshall, "JCSDA Community Radiative Transfer Model (CRTM)," in *Proc. 14th TOVS Conf.*, Beijing, China, 2005.

[28] B. Yan and F. Weng, "Assessments of F16 Special Sensor Microwave Imager and sounder antenna temperatures at lower atmospheric sounding channels," *Adv. Meteorol.*, vol. 2009, pp. 1–18, 2009, Article ID 420985.

Sid-Ahmed Boukabara received the Engineer degree in signal processing from the National School of Aeronautics (ENAC), Toulouse, France, in 1994, the M.S. degree in signal processing from the Institut National Polytechnique de Toulouse, Toulouse, in 1994, and the Ph.D. degree in remote sensing from the Denis Diderot University, Paris, France, in 1997.

He was involved in the calibration/validation of the European Space Agency's ERS-2 microwave radiometer, and he has worked on the synergistic use of active and passive microwave measurements. He joined AER Inc., Cambridge, MA, in 1998 and worked on the design, implementation, and validation of the National Polar-orbiting Operational Environmental Satellite System (NPOESS)/Conical-Scanning Microwave Imager/Sounder physical retrieval algorithm on the NASA SeaWinds/QuikSCAT wind vector rain flag and on the development of the atmospheric absorption model MonoRTM, dedicated to the microwave and laser applications. In 2005, he joined the National Oceanic and Atmospheric Administration/National Environmental Satellite, Data, and Information Service, Camp Springs, MD, and since then, he has been leading an effort to develop the capability of assimilating passive microwave measurements in all-weather conditions using a combination of variational technique algorithm and the Community Radiative Transfer Model. In 2009, he was nominated as the Deputy Director of the Joint Center for Satellite Data Assimilation. His principal areas of interest include radiative transfer modeling, including absorption and scattering of the surface and the atmosphere; spectroscopy; algorithm development using neural networks; assimilation-type techniques; and statistical approaches.

Kevin Garrett received the M.S. degree in atmospheric sciences from Texas A&M University, College Station, in 2007.

He joined the I.M. Systems Group, Inc., National Oceanic and Atmospheric Administration (NOAA)/National Environmental Satellite, Data, and Information Service, Camp Springs, MD, as a Support Scientist. His primary effort is focused on the development of passive microwave remote sensing retrieval algorithms, and he is currently leading the effort of integrating NOAA's Microwave Integrated Retrieval System within the NPOESS Data Exploitation operational environment.

Wanchun Chen received the M.S. degree in meteorology from the University of Maryland, College Park, in 2000 and the M.S. degree in computer sciences from Johns Hopkins University, Baltimore, MD, in 2005.

He is with Dell, Inc., in support of the Microwave Integrated Remote Systems as a System Developer and as a Web Developer with the Center for Satellite Applications and Research, National Environmental Satellite, Data, and Information Service, National Oceanic and Atmospheric Administration, Camp Springs, MD.

This article has been accepted for inclusion in a future issue of this journal. Content is final as presented, with the exception of pagination.

Flavio Iturbide-Sanchez (S'03–M'07) received the B.S.E.E. degree in electronics engineering from the Autonomous Metropolitan University, Mexico City, Mexico, in 1999, the M.S.E.E. degree in electrical engineering from the Advanced Studies and Research Center, National Polytechnic Institute, Mexico City, in 2001, and the Ph.D. degree from the University of Massachusetts, Amherst, in 2007, where he was advised by Prof. S. C. Reising and supported by the National Science Foundation.

His Ph.D. research focused on the miniaturization, development, calibration, and performance assessment of low-cost and power-efficient microwave radiometers for remote sensing applications. From 2001 to 2005, he was a Research Assistant with the Microwave Remote Sensing Laboratory, University of Massachusetts, where he performed research on the design, development, and characterization of highly integrated multichip modules and microwave circuits for low-noise, low-power consumption, high-gain, and high-stability microwave radiometers. From 2005 to 2007, he was with the Microwave Systems Laboratory, Colorado State University, Fort Collins, focusing on the design, testing, deployment, and data analysis of the low-cost and power-efficient Compact Microwave Radiometer for Humidity Profiling. Since 2008, he has been with the I.M. Systems Group, Inc., National Oceanic and Atmospheric Administration/National Environmental Satellite, Data, and Information Service/Center for Satellite Applications and Research, Camp Springs, MD. His research interests include communication systems; microwave radiometry; microwave/millimeter-wave IC design and packaging; RF integrated circuits; system-on-a-chip; active antennas; modeling, analysis, design, and measurement of microwave and millimeter-wave circuits and systems; and atmospheric remote sensing, including retrieval algorithm development.

Dr. Iturbide-Sanchez received the First-Place Poster Award at the 11th Specialist Meeting on Microwave Radiometry and Remote Sensing Applications (MicroRad 2010) in Washington, DC. While he was a Ph.D. student, he was a finalist in two IEEE Student Paper Competitions: one at the International Geoscience and Remote Sensing Symposium in Anchorage, AK, in September 2004 and one at the International Microwave Symposium in San Francisco, CA, in June 2006. He was also awarded the Mexican National Council for Science and Technology (CONACYT) Graduate Fellowship from 1999 to 2004.

Christopher Grassotti received the B.S. degree in earth and space science from the State University of New York, Stony Brook, the M.S. degree in atmospheric science from the University of Wisconsin, Madison, and the M.S. degree in viticulture and enology from the Ecole Nationale Superieure Agronomique (now SupAgro), Montpellier, France.

He has previously worked for Atmospheric and Environmental Research, Inc., Lexington, MA, and Environment Canada, Montreal, QC, Canada. He is currently with the I.M. Systems Group, Inc., Camp Springs, MD, as a Contractor for the National Oceanic and Atmospheric Administration/National Environmental Satellite, Data, and Information Service/Center for Satellite Applications and Research, focusing on the development and improvements in the Microwave Integrated Retrieval System.

Cezar Kongoli received the M.Sc. degree in soil and water from Wageningen University, Wageningen, The Netherlands, in 1994 and the Ph.D. degree in environmental biophysics from the University of Wisconsin, Madison, in 2000.

Since 2000, he has been with the National Oceanic and Atmospheric Administration/National Environmental Satellite, Data, and Information Service, Camp Springs, MD, working on the development of satellite remote sensing algorithms, with an emphasis on snow and ice. His work has included the development of the Advanced Microwave Sounding Unit (AMSU) based falling snow and snow cover algorithms and, more recently, the development of advanced snow cover and sea ice algorithms from variationally retrieved surface emissivities using AMSU/MHS and SSMI/S observations. He is currently an Assistant Research Scientist with the Earth System Science Interdisciplinary Center, University of Maryland, College Park.

Ruiyue Chen received the B.S. and M.S. degrees in electrical engineering from the Nanjing University of Aeronautics and Astronautics, Nanjing, China, in 1997 and 2000, respectively, the M.S. degree in atmospheric sciences from Texas A&M University, College Station, in 2003, and the Ph.D. degree in atmospheric sciences from the University of Maryland, College Park, in 2010.

In 2007, he joined the I.M. Systems Group, Inc., Rockville, MD, in support of satellite remote sensing and sensor calibration for the National Oceanic and Atmospheric Administration/National Environmental Satellite, Data, and Information Service. His principal areas of interest include microwave remote sensing and satellite sensor calibration.

Quanhua Liu received the B.S. degree from the Nanjing Institute of Meteorology, Nanjing, China, in 1981, the M.S. degree in physics from the Chinese Academy of Sciences, Beijing, China, in 1984, and the Ph.D. degree in marine science from the University of Kiel, Kiel, Germany, in 1991.

He is with the Joint Center for Satellite Data Assimilation, Camp Springs, MD. His primary interests are radiative transfer theory, retrieval methodology, solar and wind energy assessment, and prediction and applications of satellite data.

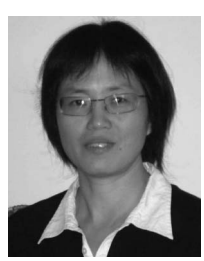

Banghua Yan received the Ph.D. degree in atmospheric physics from the Institute of Atmospheric Physics, Chinese Academy of Sciences, Beijing, China, in 1997 and the Ph.D. degree in atmospheric and ocean remote sensing from the University of Alaska, Fairbanks, in 2001.

Since November 1999, she has been with the National Oceanic and Atmospheric Administration (NOAA)/National Environmental Satellite, Data, and Information Service/Center for Satellite Applications and Research, Camp Springs, MD. She was an Associate Research Scientist with the Earth System Science Interdisciplinary Center, University of Maryland, College Park, and the Joint Center for Satellite Data Assimilation (JCSDA), NOAA, Camp Springs. She is currently with the Office of Satellite Data Processing and Distribution, NOAA, as an Oceanographer. In the past few years, she directly contributed in the developments of microwave land, snow, and sea ice emissivity models which have significantly improved uses of satellite sounding data in numerical weather prediction (NWP) models and have impacted the high-latitude weather forecasts. These land, snow, and sea ice microwave emissivity models have been implemented into the NOAA NCEP NWP model and the JCSDA Community Radiative Transfer Model that has been successfully used in several operational data assimilation systems in the U.S. The major fields she is working on include the following: 1) land and snow microwave emissivity modeling and retrievals; 2) assimilation impacts of microwave satellite measurements on global NWP models; and 3) remote sensing of ocean color. She has published over 15 papers in international peer-reviewed journals in the past several years.

This article has been accepted for inclusion in a future issue of this journal. Content is final as presented, with the exception of pagination.

Fuzhong Weng received the Ph.D. degree from the Department of Atmospheric Science, Colorado State University, Fort Collins, in 1992.

He is the Chief of the Satellite Calibration and Data Assimilation Branch, National Oceanic and Atmospheric Administration (NOAA)/National Environmental Satellite, Data, and Information Service/Center for Satellite Applications and Research, Camp Springs, MD. In the past years, he has been leading the developments of NOAA operational satellite microwave products and algorithms from the Special Sensor Microwave Imager and Advanced Microwave Sounding Unit. He is the Sensor Science Chair of the NPP/JPSS program. He is a Science Lead in developing the Community Radiative Transfer Model that has been successfully used in several operational data assimilation systems in the U.S. He also directly contributed in the developments of microwave land, snow, and sea ice emissivity models which have significantly improved uses of satellite sounding data in numerical weather prediction (NWP) models and have impacted the high-latitude weather forecasts. He is currently developing new innovative techniques to advance uses of satellite measurements under cloudy and precipitation areas in NWP models.

Dr. Weng was the first winner of the 2000 NOAA David Johnson Award for his outstanding contributions to satellite microwave remote sensing fields and the utilization of satellite data in the NWP models. He also received the 2002 SPIE Scientific Achievement Award for Excellence in Developing Operational Satellite Microwave Products and Algorithms. He was awarded in 2004 by the U.S. Department of Commerce with a bronze medal for his developments of operational microwave products to improve weather and climate predictions. He was the winner of the Department of Commerce Gold Medal Award in 2005 for his achievement in satellite data assimilation, and he also received the NOAA bronze medal for leading successful NOAA-18 instrument calibration.

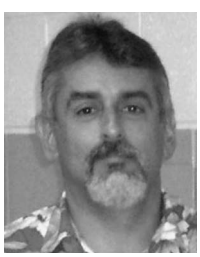

Ralph Ferraro received the B.S. degree in meteorology from Rutgers University, Camden, NJ, in 1980 and the M.S. degree in meteorology from the University of Maryland, College Park, in 1982.

He is the Chief of the Satellite Climate Studies Branch, National Oceanic and Atmospheric Administration (NOAA)/National Environmental Satellite, Data, and Information Service, College Park, MD. His research focuses on the use of environmental satellite remote sensing for both weather and climate studies, with an emphasis on precipitation and other hydrological cycle products. He is a member of NASA's Precipitation Measurement Missions and AMSR-E science teams and the Cochair of the NOAA's Steering Group on Precipitation Measurement from Space. He is the former Cochair of the International Precipitation Working Group.

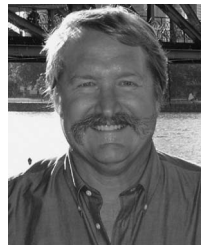

Thomas J. Kleespies received the B.S. degree in atmospheric sciences from the University of Washington, Seattle, in 1974, the M.S. degree in atmospheric from Colorado State University, Fort Collins, in 1977, and the Ph.D. degree in meteorology from The University of Utah, Salt Lake City, in 1994.

He was employed by the Naval Environmental Prediction Research Facility as a Research Meteorologist from 1978 to 1984. He was employed by the Air Force Geophysics Laboratory as a Research Meteorologist from 1984 to 1993. Since 1993, he has been a Physical Scientist with the National Oceanographic and Atmospheric Administration/National Environmental Satellite, Data, and Information Service, Camp Springs, MD. At the end of December 2010, he retired after more than 33 years of federal service.

Dr. Kleespies is a member of the American Meteorological Society, the American Association for the Advancement of Science, the American Geophysical Union, and the Optical Society of America. He has received several Department of Commerce medals for superior and meritorious service.

Huan Meng received the M.S. degree in physical oceanography from Florida State University, Tallahassee, in 1993 and the Ph.D. degree in hydrology from Colorado State University, Fort Collins, in 2004.

She is currently a Physical Scientist with the National Oceanic and Atmospheric Administration (NOAA)'s National Environmental Satellite, Data, and Information Service (NESDIS), College Park, MD. Her main areas of interest are in developing snowfall rate retrieval algorithm and climate data record, both using measurements from satellite-based passive microwave radiometers. Prior to the current position, she was with QSS Group, Inc., and supported NESDIS from 1999 to 2006.